Journal of Computational Physics 269 (2014) 355–385

Contents lists available at ScienceDirect

Journal of Computational Physics

www.elsevier.com/locate/jcp

High order weighted essentially nonoscillatory WENO-η schemes for hyperbolic conservation laws

Ping Fan [a,b]

[a] Institute of Process Engineering, Chinese Academy of Sciences, Beijing 100190, China
[b] Institute of Mechanics, Chinese Academy of Sciences, Beijing 100190, China

ARTICLE INFO

Article history:
Received 25 October 2013
Received in revised form 10 March 2014
Accepted 14 March 2014
Available online 31 March 2014

Keywords:
Weighted essentially non-oscillatory
WENO-Z
WENO-η
WENO-Zη
Smoothness indicators
High order accuracy

ABSTRACT

In [8], the authors have designed a new fifth-order WENO finite-difference scheme (named WENO-η) by introducing a new local smoothness indicator which is defined based on the Lagrangian interpolation polynomials and has a more succinct form compared with the classical one proposed by Jiang and Shu [12]. With this new local smoothness indicator, higher order global smoothness indicators were able to be devised and the corresponding scheme (named WENO-Zη) displayed less numerical dissipations than the classic fifth-order WENO schemes, including WENO-JS [12] and WENO-Z [5,6]. In this paper, a close look is taken at Taylor expansions of the Lagrangian interpolation polynomials of the WENO sub-stencils and the related inherited symmetries of the local smoothness indicators, which allows the extension of the WENO-η scheme to higher orders of accuracy. Furthermore, general formulae for the global smoothness indicators are derived with which the WENO-Zη schemes can be extended to all odd-orders of accuracy. Numerical experiments are conducted to demonstrate the performance of the proposed schemes.

1. Introduction

High-order accurate weighted essentially non-oscillatory (WENO) schemes have recently been developed to solve the hyperbolic conservation law

$$u_t + f(u)_x = 0 \tag{1}$$

Based on the successful essentially non-oscillatory (ENO) scheme in [10], WENO schemes use the idea of adaptive stencils in the reconstruction procedure to automatically achieve high-order accuracy and non-oscillatory property near discontinuities [15]. The first WENO scheme was developed by Liu, Osher and Chan [14] for a third-order of accuracy and the classic fifth-order WENO scheme with a general framework for the design of the smoothness indicators and nonlinear weights was constructed in [12] which will be referred hereafter as WENO-JS. Later, very high order WENO schemes were developed in [1] and [9].

WENO schemes use a nonlinear convex combination of all the ENO candidate sub-stencils and assign each sub-stencil a weight between 0 and 1 based on local smoothness indicators. In smooth regions of the solution, the WENO methodology uses optimal weights for each of the lower order polynomials to achieve in combining an upwind scheme of maximum order. On the other hand, small weights are assigned to the lower order polynomials whose underlying stencils contain

E-mail addresses: pfan@ipe.ac.cn, fanping@imech.ac.cn.

http://dx.doi.org/10.1016/j.jcp.2014.03.033
0021-9991/

discontinuities so that the ENO property is ensured. The first set of nonlinear weights of widespread use has been presented in the WENO-JS scheme, in which β is the associated local smoothness indicator. In [11], it was demonstrated that the smoothness indicator of WENO-JS failed to recover the maximum order of the scheme at critical points where the first or higher order derivatives of the function vanished. In the same paper, they proposed a new WENO-M scheme to fix this problem by modifying the smoothness indicator of WENO-JS with a mapping procedure to satisfy the sufficient criteria for fifth-order convergence. With a different weighting formulation, Borges, Carmona, Costa and Don [5] introduced another version of the fifth-order WENO scheme (called WENO-Z) which uses a global higher order reference value for the smoothness indicators and drives the WENO weights to the optimal values faster than the WENO-M scheme. The WENO-Z presents a less dissipation than WENO-JS but at the first order critical points the convergence order is 4th and will degrade to 2nd when higher order critical points are met. In [6], a closed-form formula for the WENO-Z scheme of higher than fifth-order accuracy was derived.

Recently, developments have also been made in designing WENO schemes on unstructured meshes in more space dimensions. For example, a third-order finite volume WENO scheme was constructed on three dimensional tetrahedral meshes [18] and an arbitrary high order finite volume WENO scheme on unstructured grids in two and three space dimensions was developed by using the ADER (ADER stands for Arbitrary Derivative Riemann problem) approach [7]. In [13] a third-order compact central WENO scheme was presented for multidimensional conservation laws.

Excepting applications for the hydrodynamics problems, the WENO schemes have also been applied for solving the magnetohydrodynamics (MHD) problems. For example, the divergence-free WENO schemes for simulating the MHD flows were designed by Balsara [2] and it was found that for MHD the ADER-WENO schemes are better than the Runge–Kutta (*RK*)-WENO schemes. In [3,4] efficient techniques for WENO interpolation have been proposed in developing the ADER-WENO schemes for the divergence-free MHD. They presented very elegant and compact formulations of WENO reconstruction as well as their implementation details by expressing the interpolating functions in modal space of Hermite polynomial.

In [8], the authors developed a new fifth-order WENO scheme (named WENO-η) by introducing a new smoothness indicator η which is defined based on the Lagrangian interpolation polynomial and has a more succinct form compared with the classical one of WENO-JS. With the new smoothness indicator η, several new global smoothness indicators τ_{2r-1} can be designed and optimized to 8th-order and the associated WENO scheme, named WENO-Zη, can achieve fifth-order convergence rate in smooth regions (even at the second order critical points where the first and second derivatives vanish). It was observed from the presented numerical results that the numerical dissipation of WENO-η scheme is equivalent to WENO-JS, while, the WENO-Zη scheme with the optimized global smoothness indicator τ_{2r-1} is less dissipative than the other WENO schemes.

In this article, the fifth order WENO-η and WENO-Zη schemes introduced in [8] are extended to higher orders of accuracy by deriving the corresponding explicit formulae of the local smoothness indicator η and providing a closed-form formula for the generation of the global smoothness indicators τ_{2r-1}. A thorough examination of the Taylor expansions of the Lagrangian interpolation polynomials reveals that the Lagrangian interpolation bases of the local sub-stencils are symmetrical with respect to the global stencil, and, accordingly, the local smoothness indicators η_l have similar symmetries and can be used via linear combinations of η to build τ_{2r-1} for all values of r. Moreover, it is found that the order of the global smoothness indicator τ_{2r-1} can be optimized from $r+2$ to $2r+2$ through using instead of η but the derivatives of the Lagrangian interpolation polynomials directly. The rest of this paper is organized as follows. In Section 2, a brief review of the WENO schemes is given. The main result of this paper will be presented in Section 3, where we derive the explicit expressions of the local smoothness indicator η and the general formula for the higher order global smoothness indicators τ_{2r-1} of all odd orders WENO-Zη schemes. Section 4 presents the accuracy test for the developed scheme. Numerical results are run in Section 5 to distinguish WENO-η and WENO-Zη with the classic WENO schemes. Section 6 concludes this paper.

2. Review of the WENO schemes

For the hyperbolic conservation law (1), the flux function $f(u)$ is split into two parts as $f(u) = f^+(u) + f^-(u)$ with $\mathrm{d}f^+(u)/\mathrm{d}u \geqslant 0$ and $\mathrm{d}f^-(u)/\mathrm{d}u \leqslant 0$. The semi-dicretization form of (1) can be written as

$$\frac{\mathrm{d}u_i(t)}{\mathrm{d}t} = -\frac{1}{\Delta x}(h_{i+\frac{1}{2}} - h_{i-\frac{1}{2}}), \tag{2}$$

where the numerical flux is $h_{i+1/2} = h_{i+1/2}{}^+ + h_{i+1/2}{}^-$. Hereinafter, only the positive part $h_{i+1/2}{}^+$ is described and the superscript "+" is dropped for simplicity.

The flux of the classical $(2r-1)$th-order WENO-JS scheme is built through the convex combination of interpolated values $R_{i-r+1+l,r}(x_{i+1/2})$ $(l = 0, 1, \ldots, r-1)$

$$h_{i+\frac{1}{2}} = \sum_{l=0}^{r-1} \omega_{l,r} R_{i-r+1+l,r}(x_{i+\frac{1}{2}}) + O\left(\Delta x^{2r-1}\right), \tag{3}$$

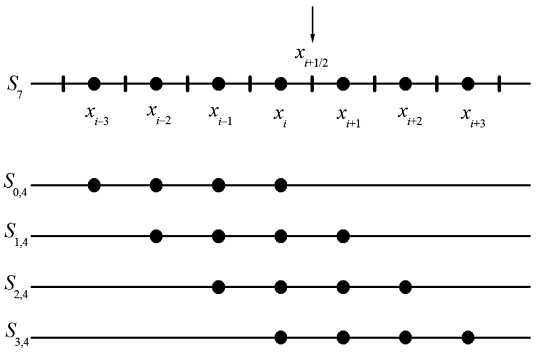

Fig. 1. The computational uniform grid x_i and the 7-points stencil S_7, composed of four 4-points stencils $S_{0,4}$, $S_{1,4}$, $S_{2,4}$, and $S_{3,4}$, used for the seventh-order WENO reconstruction step.

in which $R_{i-r+1+l,r}$ is the reconstruction polynomial on point stencil $S_{l,r} = \{I_{i-r+1+l}, I_{i-r+2+l}, \ldots, I_{i+l}\}$ $(I_i \equiv \{x_{i-1/2}, x_{i+1/2}\})$

$$R_{i-r+1+l,r}(x_{i+\frac{1}{2}}) = \sum_{m=0}^{r-1} c_{lm,r} f_{i-r+1+l+m}, \quad i = 0, \ldots, N \tag{4}$$

Fig. 1 presents the computational uniform grid x_i and the point stencils $S_{l,r}$ for $r = 4$. The coefficients $(\mathbf{c}_{lm,r})$ for $r = 3$ and 4 read [1]

$$(\mathbf{c}_{lm,3}) = \begin{pmatrix} c_{00,3} & c_{01,3} & c_{02,3} \\ c_{10,3} & c_{11,3} & c_{12,3} \\ c_{20,3} & c_{21,3} & c_{22,3} \end{pmatrix} = \begin{pmatrix} \frac{1}{3} & -\frac{7}{6} & \frac{11}{6} \\ -\frac{1}{6} & \frac{5}{6} & \frac{1}{3} \\ \frac{1}{3} & \frac{5}{6} & -\frac{1}{6} \end{pmatrix} \tag{5}$$

$$(\mathbf{c}_{lm,4}) = \begin{pmatrix} c_{00,4} & c_{01,4} & c_{02,4} & c_{03,4} \\ c_{10,4} & c_{11,4} & c_{12,4} & c_{13,4} \\ c_{20,4} & c_{21,4} & c_{22,4} & c_{23,4} \\ c_{30,4} & c_{31,4} & c_{32,4} & c_{33,4} \end{pmatrix} = \begin{pmatrix} -\frac{1}{4} & \frac{13}{12} & -\frac{23}{12} & \frac{25}{12} \\ \frac{1}{12} & -\frac{5}{12} & \frac{13}{12} & \frac{1}{4} \\ -\frac{1}{12} & \frac{7}{12} & \frac{7}{12} & -\frac{1}{12} \\ \frac{1}{4} & \frac{13}{12} & -\frac{5}{12} & \frac{1}{12} \end{pmatrix} \tag{6}$$

It should be mentioned that Balsara et al. [3] provide a general strategy for obtaining Eqs. (5) and (6). Also, the formulae in [3] can be used to even form analogous matrices at ninth order.

The non-oscillatory weights $\omega_{l,r}$ are defined as

$$\omega_{l,r} = \frac{\alpha_l}{\sum_{m=0}^{r-1} \alpha_m}, \qquad \alpha_l = \frac{d_{l,r}}{(\varepsilon + \beta_{l,r})^p}, \tag{7}$$

where $\beta_{l,r}$ are the local smoothness indicators; $d_{l,r}$ are called the ideal weights since they generate the central upstream $(2r-1)$th-order scheme for the $(2r-1)$-points stencil $S_{i-r+1,2r-1} = \{I_{i-r+1}, \ldots, I_{i+r-1}\}$. For $r = 3$ and 4, the ideal weights are

$$\begin{cases} d_{0,3} = \frac{1}{10}; & d_{1,3} = \frac{3}{5}; & d_{2,3} = \frac{3}{10} \\ d_{0,4} = \frac{1}{35}; & d_{1,4} = \frac{12}{35}; & d_{2,4} = \frac{18}{35}; & d_{3,4} = \frac{4}{35} \end{cases} \tag{8}$$

The general idea of the weights definition (7) is that if the function $f(x)$ is smooth in all of the candidate stencils the smoothness indicators $\beta_{l,r}$ are all small and about the same size, generating weights $\omega_{l,r}$ that approximate the ideal weights $d_{l,r}$ with rth-order of accuracy. Then, the convex combination of all $R_{i-r+1+l,r}$ guarantees $(2r-1)$th-order of accuracy to approximate the flux at the cell boundary. On the other hand, if $f(x)$ has a discontinuity in the sub-stencil $S_{l,r}$ but is smooth in at least one of the other stencils, then $\beta_{l,r}$ is $O(1)$ and the corresponding weight $\omega_{l,r}$ is small relatively to the other weights. The scheme is then rth-order accurate and emulation of ENO is achieved.

Henrick, Aslam and Powers [11] indicated that to ensure the overall scheme retaining $(2r-1)$th-order accuracy, it is sufficient to require

$$\omega_{l,r}^{\pm} - d_{l,r} = O\left(\Delta x^r\right) \tag{9}$$

To meet the above requirement in the case of $r = 3$, they proposed a mapping function to make $\omega_{l,3}$ approximating the ideal weights $d_{l,3}$ with an increased accuracy. The mapping function used in the WENO-M scheme is defined as

$$g_l(\omega) = \frac{\omega(d_{l,3} + d_{l,3}^2 - 3d_{l,3}\omega + \omega^2)}{d_{l,3}^2 + \omega(1 - 2d_{l,3})} \tag{10}$$

Borges, Carmona, Costa, and Don [5] introduced the absolute difference between $\beta_{0,3}$ and $\beta_{2,3}$ to devise a new set of WENO weights

$$\omega_l^z = \frac{\alpha_l^z}{\sum_{m=0}^{2}\alpha_m^z}, \qquad \alpha_l^z = d_l\left(1 + \left(\frac{\tau_5}{\varepsilon + \beta_{l,3}}\right)^p\right), \quad l = 0, 1, 2, \tag{11}$$

where the global smoothness indicator τ_5 for measuring the smoothness of the large stencil S_5 is defined as

$$\tau_5 = |\beta_{0,3} - \beta_{2,3}| \tag{12}$$

The reader who is not interested in the proof can skip directly to the text that follows after Eq. (33). We point out that Eqs. (11) and (33) fully define the WENO-$Z\eta$ scheme. With this implementation the convex combination of the WENO-Z weights becomes closer to the central scheme than that of the WENO-JS and hence gains less dissipation. Furthermore, the computational cost is smaller than the WENO-M scheme. A general expression of the global smoothness indicator for arbitrary r was obtained by Castro, Costa, and Don [6], given by,

$$\tau_{2r-1} = \begin{cases} |\beta_{0,r} - \beta_{r-1,r}|, & \mod(r,2) = 1 \\ |\beta_{0,r} + \beta_{r-1,r} - (\beta_{1,r} + \beta_{r-2,r})|, & \mod(r,2) = 0 \end{cases} \tag{13}$$

3. The smoothness indicators of WENO-η

3.1. The classic local smoothness indicator β

The smoothness indicator that evaluates the local smoothness of a function in a stencil was defined originally in [14], which can be written as

$$IS_{l,r} = \sum_{n=1}^{r-1}\sum_{m=1}^{r-n}\frac{(f[i+l+m-r, n])^2}{r-n}, \tag{14}$$

where $[\cdot,\cdot]$ is the nth undivided difference operator. With this smoothness indicator, an $(r+1)$th-order WENO scheme is *obtained* from an rth-order ENO scheme. To improve accuracy, Jiang and Shu [12] designed a smoothness indicator as

$$\beta_{l,r} = \sum_{m=1}^{2}\Delta x^{2m-1}\int_{x_{i-\frac{1}{2}}}^{x_{i+\frac{1}{2}}}\left(\frac{d^m}{dx^m}R_{i-r+1+l,r}(x)\right)^2 dx \tag{15}$$

For $r = 4$, the explicit formulae for $\beta_{l,r}$ in terms of the cell averaged value of f can be expressed as [1]

$$\begin{cases} \beta_{0,4} = f_{i-3}(547f_{i-3} - 3882f_{i-2} + 4642f_{i-1} - 1854f_i) + f_{i-2}(7043f_{i-2} \\ \qquad - 17\,246f_{i-1} + 7042f_i) + f_{i-1}(11\,003f_{i-1} - 9402f_i) + 2107f_i^2; \\ \beta_{1,4} = f_{i-2}(267f_{i-2} - 1642f_{i-1} + 1602f_i - 494f_{i+1}) + f_{i-1}(2843f_{i-1} \\ \qquad - 5966f_i + 1922f_{i+1}) + f_i(3443f_i - 2522f_{i+1}) + 547f_{i+1}^2; \\ \beta_{2,4} = f_{i-1}(547f_{i-1} - 2522f_i + 1922f_{i+1} - 494f_{i+2}) + f_i(3443f_i \\ \qquad - 5966f_{i+1} + 1602f_{i+2}) + f_{i+1}(2843f_{i+1} - 1642f_{i+2}) + 267f_{i+2}^2; \\ \beta_{3,4} = f_i(2107f_i - 9402f_{i+1} + 7042f_{i+2} - 1854f_{i+3}) + f_{i+1}(11\,003f_{i+1} \\ \qquad - 17\,246f_{i+2} + 4642f_{i+3}) + f_{i+2}(7043f_{i+2} - 3882f_{i+3}) + 547f_{i+3}^2 \end{cases} \tag{16}$$

The smoothness indicator defined by (15) has currently been widely used in the WENO schemes, with which an rth-order ENO scheme can be converted to a $(2r-1)$th-order WENO scheme. However, to evaluate the explicit form of $\beta_{l,r}$ is essentially a very hard work, since it involves an integral calculation on the square of derivatives of the reconstruction polynomials. Although the explicit formula of $\beta_{l,r}$ for $r = 4$, 5, 6 and $r = 7$, 8, 9 have been presented by Balsara and Shu [1] and Gerolymos, Schal and Vallet [9], respectively, the works for evaluating the explicit form of $\beta_{l,r}$ are still tremendously burdensome especially for large r.

Apart from the above mentioned works on the explicit formulae for the smoothness indicator, it is worthy of a particular mention that new expressions that are more compact than those in [1] have also been obtained in [3,4] recently. By casting the problem in a modal space of Hermit polynomials

$$q_0(\xi)=1,\qquad q_1(\xi)=\xi,\qquad q_2(\xi)=\xi^2-\frac{1}{12},\qquad q_3(\xi)=\xi^3-\frac{3}{20}\xi,$$
$$q_4(\xi)=\xi^4-\frac{3}{14}\xi^2+\frac{3}{560}, \tag{17}$$

Balsara et al. [3,4] have succeeded in deriving a more elegant and compact formulation for the smoothness indicators, which can be expressed as $(r=4)$

$$IS_i=\left(f_{xi}+\frac{f_{xxxi}}{10}\right)^2+\frac{13}{3}(f_{xxi})^2+\frac{781}{20}(f_{xxxi})^2;\quad (i=0,1,2,3), \tag{18}$$

where

$$f_{x0}=\frac{1}{60}(-19f_{i-3}+87f_{i-2}-177f_{i-1}+109f_i);$$
$$f_{xx0}=\frac{1}{2}(-f_{i-3}+4f_{i-2}-5f_{i-1}+2f_i);$$
$$f_{xxx0}=\frac{1}{6}(-f_{i-3}+3f_{i-2}-3f_{i-1}+f_i) \tag{19}$$
$$f_{x1}=\frac{1}{60}(11f_{i-2}-63f_{i-1}+33f_i+19f_{i+1});$$
$$f_{xx1}=\frac{1}{2}(f_{i-1}-2f_i+f_{i+1});$$
$$f_{xxx1}=\frac{1}{6}(-f_{i-2}+3f_{i-1}-3f_i+f_{i+1}) \tag{20}$$
$$f_{x2}=\frac{1}{60}(-19f_{i-1}-33f_i+63f_{i+1}-11f_{i+2});$$
$$f_{xx2}=\frac{1}{2}(f_{i-1}-2f_i+f_{i+1});$$
$$f_{xxx2}=\frac{1}{6}(-f_{i-1}+3f_i-3f_{i+1}+f_{i+2}) \tag{21}$$
$$f_{x3}=\frac{1}{60}(-109f_i+177f_{i+1}-87f_{i+2}+19f_{i+3});$$
$$f_{xx3}=\frac{1}{2}(2f_i-5f_{i+1}+4f_{i+2}-f_{i+3});$$
$$f_{xxx3}=\frac{1}{6}(-f_i+3f_{i+1}-3f_{i+2}+f_{i+3}) \tag{22}$$

3.2. The local smoothness indicator η

In [8], a new succinct formula for the local smoothness indicators are presented, defined by

$$\eta_{l,r}=\sum_{m=1}^{r-1}\left[\Delta x^m P^{(m)}_{i-r+1+l,r}(x_i)\right]^2,\quad 0\leqslant l\leqslant r-1, \tag{23}$$

where $P^{(m)}_{i,r}(x)$ is the mth derivative of the Lagrangian interpolation polynomial $P_{i,r}(x)$. For approximating the flux function f at any point x based upon an r-point stencil $S_{i,r}=\{x_i,\ldots,x_{i+r-1}\}$, the Lagrangian interpolation polynomial $P_{i,r}(x)$ is defined by

$$P_{i,r}(x)=\sum_{m=0}^{r-1}f_{i+m}\prod_{l=0,l\neq m}^{r-1}\frac{x-x_{i+l}}{x_{i+m}-x_{i+l}} \tag{24}$$

The explicit forms of $P^{(m)}_{i-r+1+l,r}(x_i)$ and $\eta_{l,r}$ for $r=3$ have been presented in [8]. In this paper, we will prove that the explicit expressions of $P^{(m)}_{i-r+1+l,r}(x_i)$ for higher order WENO-η schemes can be obtained recursively from those of the lower

order schemes. As pointed out in Appendix A, the Lagrangian interpolation polynomial $P_{i,r}(x)$ has the following recursive relation

$$P_{i,r+1}(x) = \gamma_{i,r} P_{i,r}(x) + \widehat{\gamma}_{i,r} P_{i+1,r}(x), \tag{25}$$

where

$$\gamma_{i,r} = \frac{x_{i+r} - x}{x_{i+r} - x_i}, \qquad \widehat{\gamma}_{i,r} = \frac{x - x_i}{x_{i+r} - x_i} \tag{26}$$

By taking the mth derivative on the above equation, one can have

$$P^{(m)}_{i,r+1}(x) = \gamma_{i,r} P^{(m)}_{i,r}(x) + \widehat{\gamma}_{i,r} P^{(m)}_{i+1,r}(x) + m \frac{P^{(m-1)}_{i+1,r}(x) - P^{(m-1)}_{i,r}(x)}{x_{i+r} - x_i} \tag{27}$$

With aid of the above recursive relation, the explicit forms of $P^{(m)}_{i-r+1+l,r}(x_i)$ for r greater than 3 can be derived recursively from the known results of $r = 3$ (details of the derivations can be found in Appendix C). This property of Lagrangian interpolation polynomials can significantly simplify derivations of the explicit expressions of $\eta_{l,r}$ for greater r and can hence be regarded as another advantage over the currently prevalent formulae of $\beta_{l,r}$. In what follows, we shall list the results for $r = 4$ and those for $r = 5$ and $r = 6$ are presented in Appendix C. The derivatives of the Lagrangian interpolation polynomials for $r = 4$ are given by $(0 \leqslant l \leqslant 3)$

$$P^{(1)}_{i-l,4} = \frac{1}{6\Delta x} \sum_{n=0}^{3} s^{(1)}_{n,l,4} f_{i+n-l}; \qquad P^{(2)}_{i-l,4} = \frac{1}{\Delta x^2} \sum_{n=0}^{3} s^{(2)}_{n,l,4} f_{i+n-l};$$
$$P^{(3)}_{i-l,4} = \frac{1}{\Delta x^3} \sum_{n=0}^{3} s^{(3)}_{n,l,4} f_{i+n-l}, \tag{28}$$

where

$$\left(\mathbf{s}^{(1)}_{n,3,4}\right) = (-2, 9, -18, 11); \qquad \left(\mathbf{s}^{(1)}_{n,2,4}\right) = (1, -6, 3, 2);$$
$$\left(\mathbf{s}^{(1)}_{n,1,4}\right) = (-2, -3, 6, -1); \qquad \left(\mathbf{s}^{(1)}_{n,0,4}\right) = (-11, 18, -9, 2) \tag{29}$$
$$\left(\mathbf{s}^{(2)}_{n,3,4}\right) = (-1, 4, -5, 2); \qquad \left(\mathbf{s}^{(2)}_{n,2,4}\right) = (0, 1, -2, 1);$$
$$\left(\mathbf{s}^{(2)}_{n,1,4}\right) = (1, -2, 1, 0); \qquad \left(\mathbf{s}^{(2)}_{n,0,4}\right) = (2, -5, 4, -1) \tag{30}$$
$$\left(\mathbf{s}^{(3)}_{n,l,4}\right) = (-1, 3, -3, 1) \tag{31}$$
$$\left(\mathbf{s}^{(4)}_{n,l,5}\right) = (1, -4, 6, -4, 1) \tag{32}$$

It is seen that the above explicit expressions for $\eta_{l,r}$ from the derivatives of the Lagrangian interpolation polynomials are much more compact than the classic ones obtained by Balsara and Shu [1] and equivalently succinct as those of Balsara et al. [3,4]. Furthermore, it deserves a more particular stress that derivations for $\eta_{l,r}$ of greater r can be performed recursively from the given results of smaller r, which is much more convenient compared to the classic ways in [12] and [1].

In addition to the above two basic advantages of the new local smoothness indicator η, we will prove in the following sub-section that global smoothness indicators τ_{2r-1} can be constructed with a simple algebraic combination on η and optimized to an increased order by using the Lagrangian interpolation polynomials straightforwardly. In the case of fifth-order WENO scheme, it has been shown in [8] that the introduction of the optimized global smoothness indicator has significantly improved the 5th-order WENO scheme by decreasing the dissipations near the discontinuities and relieving the convergence problems at critical points.

3.3. The optimized global smoothness indicator τ_{2r-1}

3.3.1. Recovery of the classic τ_{2r-1}

The novel idea of the WENO-Z scheme introduced in [5,6] is the construction of the higher order global smoothness indicator τ_{2r-1} from the classic local smoothness indicator β. In this paper, we find that the general formula for the global smoothness indicator τ_{2r-1} of WENO-Z can be recovered with the newly introduced local smoothness indicator η. Similar as WENO-Z scheme in [6], the general formula for τ_{2r-1} of WENO-η scheme can be defined as $(r > 2)$

$$\tau_{2r-1} = \begin{cases} |\eta_{0,r} - \eta_{r-1,r}|, & \mod(r,2) = 1 \\ |\eta_{0,r} + \eta_{r-1,r} - (\eta_{1,r} + \eta_{r-2,r})|, & \mod(r,2) = 0 \end{cases} \tag{33}$$

Below, we will prove that the truncation error of τ_{2r-1} constituted by η is also of the order

$$\tau_{2r-1} = O\left(\Delta x^{r+2}\right), \tag{34}$$

based on the symmetric behavior of η.

Proof. In Appendices A and B, it has been proved that the Lagrangian interpolation polynomial that approximates value of a smooth function $f(x)$ at any point x based upon an r-point stencil $S_{i,r} = \{x_i, \ldots, x_{i+r-1}\}$ can be expanded as

$$P_{i,r}(x) = f(x) - \frac{f^{(r)}}{r!}\prod_{m=0}^{r-1}(x - x_{i+m}) + \frac{f^{(r+1)}}{(r+1)!}\sum_{l=0}^{r-1}(x - x_{i+l})\prod_{m=0}^{r-1}(x - x_{i+m}) + O\left(\Delta x^{r+2}\right) \tag{35}$$

From taking the nth-order derivative on the above equation, one can have

$$\begin{cases} P_{i,r}^{(1)}(x) = f^{(1)} - \dfrac{f^{(r)}}{r!}\displaystyle\sum_{l=0}^{r-1}\prod_{\substack{m=0,\\ m\neq l}}^{r-1}(x - x_{i+m}) \\ \qquad\qquad + \dfrac{f^{(r+1)}}{(r+1)!}\left[\displaystyle\sum_{j=0}^{r-1}(x - x_{i+j})\sum_{l=0}^{r-1}\prod_{\substack{m=0,\\ m\neq l}}^{r-1}(x - x_{i+m}) - \prod_{m=0}^{r-1}(x - x_{i+m})\right] + O\left(\Delta x^{r+1}\right); \\ P_{i,r}^{(2)}(x) = f^{(2)} - \dfrac{f^{(r)}}{r!}\displaystyle\sum_{j=0}^{r-1}\sum_{\substack{l=0,\\ l\neq j}}^{r-1}\prod_{\substack{m=0,\\ m\neq j,l}}^{r-1}(x - x_{i+m}) + O\left(\Delta x^{r-1}\right); \\ P_{i,r}^{(n)}(x) = f^{(n)} + O\left(\Delta x^{r-n}\right), \quad 2 < n < r \end{cases} \tag{36}$$

It will be shown in what follows that the nth-order derivative of the Lagrangian interpolation polynomial has a symmetric or asymmetric behavior with respect to the geometric disposition of the point stencils, and based on which the higher order global smoothness indicators can be devised accordingly.

Firstly, one can deduce from (36) the Taylor series expansion for the 1st-order derivative of the Lagrangian interpolation polynomial under the uniform grid approximation (which will be implemented throughout this paper), given by

$$P_{i-r+l,r}^{(1)}(x_i) = f_i^{(1)} + \sum_{s=r-1}^{r} C_{p,s}^{(1)}(l)\Delta x^s + O\left(\Delta x^{r+1}\right), \quad 1 \leqslant l \leqslant r, \tag{37}$$

where the coefficients for Δx^{r-1} and Δx^r are

$$\begin{cases} C_{p,r-1}^{(1)}(l) = (-1)^l(r-l)!(l-1)!\dfrac{f_i^{(r)}}{r!}; \\ C_{p,r}^{(1)}(l) = (-1)^{l-1}\left(\displaystyle\sum_{m=1}^{r-l} m - \sum_{n=1}^{l-1} n\right)(r-l)!(l-1)!\dfrac{f_i^{(r+1)}}{(r+1)!} \end{cases} \tag{38}$$

It is readily noted that the above coefficients have the following symmetric properties

$$\begin{cases} C_{p,r-1}^{(1)}(l) = (-1)^{r-1}C_{p,r-1}^{(1)}(r-l+1), \\ C_{p,r}^{(1)}(l) = (-1)^r C_{p,r}^{(1)}(r-l+1) \end{cases} \tag{39}$$

More specifically, the explicit forms of (37) for $l = 1$, 2 and 3 can be written as

$$\begin{cases} P_{i-r+1,r}^{(1)}(x_i) = f_i^{(1)} - \dfrac{f_i^{(r)}}{r}\Delta x^{r-1} + \dfrac{r-1}{2(r+1)}f_i^{(r+1)}\Delta x^r + O\left(\Delta x^{r+1}\right); \\ P_{i-r+2,r}^{(1)}(x_i) = f_i^{(1)} + \dfrac{f_i^{(r)}}{r(r-1)}\Delta x^{r-1} - \dfrac{(r-1)(r-2)-2}{2(r+1)r(r-1)}f_i^{(r+1)}\Delta x^r + O\left(\Delta x^{r+1}\right); \\ P_{i-r+3,r}^{(1)}(x_i) = f_i^{(1)} - \dfrac{2f_i^{(r)}\Delta x^{r-1}}{r(r-1)(r-2)} + \dfrac{(r-2)(r-3)-6}{(r+1)r(r-1)(r-2)}f_i^{(r+1)}\Delta x^r + O\left(\Delta x^{r+1}\right), \end{cases} \tag{40}$$

and those for $l=r-2, r-1$ and r are

$$\begin{cases} P^{(1)}_{i-2,r}(x_i) = f_i^{(1)} - (-1)^{r-1}\dfrac{2f_i^{(r)}\Delta x^{r-1}}{r(r-1)(r-2)} + (-1)^r\dfrac{(r-2)(r-3)-6}{(r+1)r(r-1)(r-2)}f_i^{(r+1)}\Delta x^r + O\left(\Delta x^{r+1}\right); \\ P^{(1)}_{i-1,r}(x_i) = f_i^{(1)} + (-1)^{r-1}\dfrac{f_i^{(r)}}{r(r-1)}\Delta x^{r-1} - (-1)^r\dfrac{(r-1)(r-2)-2}{2(r+1)r(r-1)}f_i^{(r+1)}\Delta x^r + O\left(\Delta x^{r+1}\right); \\ P^{(1)}_{i,r}(x_i) = f_i^{(1)} - (-1)^{r-1}\dfrac{f_i^{(r)}}{r}\Delta x^{r-1} + (-1)^r\dfrac{r-1}{2(r+1)}f_i^{(r+1)}\Delta x^r + O\left(\Delta x^{r+1}\right) \end{cases} \tag{41}$$

Similarly, the Taylor series expansion for the 2nd-order derivative of the Lagrangian interpolation polynomial under the uniform grid approximation can be written as

$$P^{(2)}_{i-r+l,r}(x_i) = f_i^{(2)} + C^{(2)}_{p,r-2}(l)\Delta x^{r-2} + O\left(\Delta x^{r-1}\right), \quad 1 \leqslant l \leqslant r, \tag{42}$$

where the coefficient for Δx^{r-2} is given by

$$C^{(2)}_{p,r-2}(l) = (-1)^l 2\left(\sum_{n=1}^{r-l}\frac{1}{n} - \sum_{m=1}^{l-1}\frac{1}{m}\right)(r-l)!(l-1)!\frac{f_i^{(r)}}{r!} \tag{43}$$

Note that the above coefficient has the following symmetric property

$$C^{(2)}_{p,r-2}(l) = (-1)^r C^{(2)}_{p,r-2}(r-l+1) \tag{44}$$

For $l=1$, 2 and 3, the explicit forms of (42) can be written as

$$\begin{cases} P^{(2)}_{i-r+1,r}(x_i) = f_i^{(2)} - 2\dfrac{\sum_1^{r-1}\frac{1}{n}}{r}f_i^{(r)}\Delta x^{r-2} + O\left(\Delta x^{r-1}\right); \\ P^{(2)}_{i-r+2,r}(x_i) = f_i^{(2)} + 2\dfrac{\sum_1^{r-2}\frac{1}{n}-1}{r(r-1)}f_i^{(r)}\Delta x^{r-2} + O\left(\Delta x^{r-1}\right); \\ P^{(2)}_{i-2,r}(x_i) = f_i^{(2)} - 4\dfrac{\sum_1^{r-3}\frac{1}{n}-\frac{3}{2}}{r(r-1)(r-2)}f_i^{(r)}\Delta x^{r-2} + O\left(\Delta x^{r-1}\right), \end{cases} \tag{45}$$

and those for $l=r-2, r-1$ and r are

$$\begin{cases} P^{(2)}_{i-2,r}(x_i) = f_i^{(2)} - (-1)^r 4\dfrac{\sum_1^{r-3}\frac{1}{n}-\frac{3}{2}}{r(r-1)(r-2)}f_i^{(r)}\Delta x^{r-2} + O\left(\Delta x^{r-1}\right); \\ P^{(2)}_{i-1,r}(x_i) = f_i^{(2)} + (-1)^r 2\dfrac{\sum_1^{r-2}\frac{1}{n}-1}{r(r-1)}f_i^{(r)}\Delta x^{r-2} + O\left(\Delta x^{r-1}\right); \\ P^{(2)}_{i,r}(x_i) = f_i^{(2)} - (-1)^r 2\dfrac{\sum_1^{r-1}\frac{1}{n}}{r}f_i^{(r)}\Delta x^{r-2} + O\left(\Delta x^{r-1}\right) \end{cases} \tag{46}$$

By substituting (37) and (42) into (23), one can find that the Taylor series expansions for the local smoothness indicators $\eta_{l-1,r}$ $(1 \leqslant l \leqslant r)$ is given by

$$\eta_{l-1,r} = \sum_{m=1}^{r-1}\left[\Delta x^m P^{(m)}_{i-r+l,r}(x_i)\right]^2 = \sum_{m=1}^{r_0}\left[\Delta x^m f_i^{(m)}\right]^2 + \sum_{s=r+1}^{r+2} C_{\eta,s}(l)\Delta x^s + O\left(\Delta x^{r+3}\right), \quad 1 \leqslant l \leqslant r, \tag{47}$$

where

$$r_0 = \mathrm{int}\left(\frac{r+1}{2}\right) = \begin{cases} \frac{r+1}{2}, & \mathrm{mod}(r,2)=1; \\ \frac{r}{2}, & \mathrm{mod}(r,2)=0, \end{cases} \tag{48}$$

and the two coefficients

$$\begin{cases} C_{\eta,r+1}(l) = 2f_i^{(1)}C^{(1)}_{p,r-1}(l), \\ C_{\eta,r+2}(l) = 2f_i^{(1)}C^{(1)}_{p,r}(l) + 2f_i^{(2)}C^{(2)}_{p,r-2}(l) \end{cases} \tag{49}$$

have the following symmetrical features

$$\begin{cases} C_{\eta,r+1}(l) = (-1)^{r-1} C_{\eta,r+1}(r-l+1), \\ C_{\eta,r+2}(l) = (-1)^{r} C_{\eta,r+2}(r-l+1) \end{cases} \tag{50}$$

The explicit forms of (47) for $l = 1$, 2 and 3 are

$$\eta_{0,r} = \sum_{m=1}^{r_0} \left[\Delta x^m f_i^{(m)}\right]^2 - \frac{2}{r} f_i^{(1)} f_i^{(r)} \Delta x^{r+1} + \left[\frac{r-1}{r+1} f_i^{(1)} f_i^{(r+1)} - \frac{4\sum_{n=1}^{r-1} \frac{1}{n}}{r} f_i^{(2)} f_i^{(r)}\right] \Delta x^{r+2} + O\left(\Delta x^{r+3}\right) \tag{51}$$

$$\begin{aligned} \eta_{1,r} = {} & \sum_{m=1}^{r_0} \left[\Delta x^m f_i^{(m)}\right]^2 + \frac{2 f_i^{(1)} f_i^{(r)}}{r(r-1)} \Delta x^{r+1} \\ & + \left[-\frac{(r-1)(r-2)-2}{(r+1)r(r-1)} f_i^{(1)} f_i^{(r+1)} + 4\frac{\sum_{n=1}^{r-2} \frac{1}{n} - 1}{r(r-1)} f_i^{(2)} f_i^{(r)}\right] \Delta x^{r+2} + O\left(\Delta x^{r+3}\right) \end{aligned} \tag{52}$$

$$\begin{aligned} \eta_{2,r} = {} & \sum_{m=1}^{r_0} \left[\Delta x^m f_i^{(m)}\right]^2 - \frac{4 f_i^{(1)} f_i^{(r)}}{r(r-1)(r-2)} \Delta x^{r+1} \\ & + 2\left[\frac{(r-2)(r-3)-6}{(r+1)r(r-1)(r-2)} f_i^{(1)} f_i^{(r+1)} - 4\frac{\sum_{1}^{r-3} \frac{1}{n} - \frac{3}{2}}{r(r-1)(r-2)} f_i^{(2)} f_i^{(r)}\right] \Delta x^{r+2} + O\left(\Delta x^{r+3}\right), \end{aligned} \tag{53}$$

and those for $l = r-2, r-1$ and r are

$$\begin{aligned} \eta_{r-3,r} = {} & \sum_{m=1}^{r_0} \left[\Delta x^m f_i^{(m)}\right]^2 - (-1)^{r-1} \frac{4 f_i^{(1)} f_i^{(r)}}{r(r-1)(r-2)} \Delta x^{r+1} \\ & + (-1)^{r} 2\left[\frac{(r-2)(r-3)-6}{(r+1)r(r-1)(r-2)} f_i^{(1)} f_i^{(r+1)} - 4\frac{\sum_{1}^{r-3} \frac{1}{n} - \frac{3}{2}}{r(r-1)(r-2)} f_i^{(2)} f_i^{(r)}\right] \Delta x^{r+2} + O\left(\Delta x^{r+3}\right) \end{aligned} \tag{54}$$

$$\begin{aligned} \eta_{r-2,r} = {} & \sum_{m=1}^{r_0} \left[\Delta x^m f_i^{(m)}\right]^2 + (-1)^{r-1} \frac{2 f_i^{(1)} f_i^{(r)}}{r(r-1)} \Delta x^{r+1} \\ & + (-1)^{r} \left[-\frac{(r-1)(r-2)-2}{(r+1)r(r-1)} f_i^{(1)} f_i^{(r+1)} + 4\frac{\sum_{n=1}^{r-2} \frac{1}{n} - 1}{r(r-1)} f_i^{(2)} f_i^{(r)}\right] \Delta x^{r+2} + O\left(\Delta x^{r+3}\right) \end{aligned} \tag{55}$$

$$\begin{aligned} \eta_{r-1,r} = {} & \sum_{m=1}^{r_0} \left[\Delta x^m f_i^{(m)}\right]^2 - (-1)^{r-1} \frac{2}{r} f_i^{(1)} f_i^{(r)} \Delta x^{r+1} \\ & + (-1)^{r} \left[\frac{r-1}{r+1} f_i^{(1)} f_i^{(r+1)} - \frac{4\sum_{n=1}^{r-1} \frac{1}{n}}{r} f_i^{(2)} f_i^{(r)}\right] \Delta x^{r+2} + O\left(\Delta x^{r+3}\right) \end{aligned} \tag{56}$$

From (51), (52), (55) and (56), it is straightforward to identify that

$$\begin{cases} \mathrm{mod}\,(r,2) = 1, & \left|\eta_{0,r} - \eta_{r-1,r}\right| = O\left(\Delta x^{r+2}\right) \\ \mathrm{mod}\,(r,2) = 0, & \left|\eta_{0,r} + \eta_{r-1,r} - (\eta_{1,r} + \eta_{r-2,r})\right| = O\left(\Delta x^{r+2}\right) \end{cases}$$ □

3.3.2. The higher order $\tau_{2r-1}{}^{ho}$ ($r > 3$)

In addition to the former presented regular form for the global smoothness indicator τ_{2r-1}, it is found that τ_{2r-1} can also be formulated in another way to achieve higher order truncation error based on the symmetric feature of the local smoothness indicator η.

3.3.2.1. $\mathrm{mod}(r,2) = 0$ It can be noted from (48) and (50) that for an even r, there satisfies $r_0 = r/2$ and

$$\begin{cases} C_{\eta,r+1}(l) = -C_{\eta,r+1}(r-l+1), \\ C_{\eta,r+2}(l) = C_{\eta,r+2}(r-l+1) \end{cases} \tag{57}$$

Then, it can be derived that for $r > 3$ there should be

$$\begin{cases} \eta_{0,r} - \eta_{r-1,r} = 2C_{\eta,r+1}(1)\Delta x^{r+1} + O\left(\Delta x^{r+3}\right), \\ \eta_{1,r} - \eta_{r-2,r} = 2C_{\eta,r+1}(2)\Delta x^{r+1} + O\left(\Delta x^{r+3}\right) \end{cases} \tag{58}$$

Accordingly, a higher order global smoothness indicator ${\tau_{2r-1}}^{ho}$ can be constructed from the following way

$$\begin{aligned}{\tau_{2r-1}}^{ho} &= \left|(\eta_{0,r}-\eta_{r-1,r})-\frac{C_{\eta,r+1}(1)}{C_{\eta,r+1}(2)}(\eta_{1,r}-\eta_{r-2,r})\right| \\ &= \left|\eta_{0,r}-\eta_{r-1,r}+(r-1)(\eta_{1,r}-\eta_{r-2,r})\right| \end{aligned} \tag{59}$$

It is easy to verify that the new higher order global smoothness indicator ${\tau_{2r-1}}^{ho}$ is of the order $O(\Delta x^{r+3})$. For $r=4$, the explicit form of ${\tau_{2r-1}}^{ho}$ is written by

$${\tau_7}^{ho} = \left|\eta_{0,4}-\eta_{3,4}+3(\eta_{1,4}-\eta_{2,4})\right| \tag{60}$$

3.3.2.2. $\mathrm{mod}(r,2)=1$ From (48) and (50), it is also clear that for an odd r, there satisfies $r_0=(r+1)/2$ and

$$\begin{cases} C_{\eta,r+1}(l) = C_{\eta,r+1}(r-l+1), \\ C_{\eta,r+2}(l) = -C_{\eta,r+2}(r-l+1) \end{cases} \tag{61}$$

Thus, it can be derived that for $r>3$ there should be

$$\begin{cases} \eta_{0,r}+\eta_{r-1,r} = \sum_{m=1}^{r_0}\left[\Delta x^m f_i^{(m)}\right]^2 + 2C_{\eta,r+1}(1)\Delta x^{r+1} + O\left(\Delta x^{r+3}\right), \\ \eta_{1,r}+\eta_{r-2,r} = \sum_{m=1}^{r_0}\left[\Delta x^m f_i^{(m)}\right]^2 + 2C_{\eta,r+1}(2)\Delta x^{r+1} + O\left(\Delta x^{r+3}\right), \\ \eta_{2,r}+\eta_{r-3,r} = \sum_{m=1}^{r_0}\left[\Delta x^m f_i^{(m)}\right]^2 + 2C_{\eta,r+1}(3)\Delta x^{r+1} + O\left(\Delta x^{r+3}\right) \end{cases} \tag{62}$$

From the above equations, one can realize that

$$\left|\frac{\eta_{0,r}+\eta_{r-1,r}-\eta_{1,r}-\eta_{r-2,r}}{C_{\eta,r+1}(1)-C_{\eta,r+1}(2)} - \frac{\eta_{1,r}+\eta_{r-2,r}-\eta_{2,r}-\eta_{r-3,r}}{C_{\eta,r+1}(2)-C_{\eta,r+1}(3)}\right| = O\left(\Delta x^{r+3}\right) \tag{63}$$

Accordingly, the higher order global smoothness indicator ${\tau_{2r-1}}^{ho}$ of the order $O(\Delta x^{r+3})$ can be constructed via

$${\tau_{2r-1}}^{ho} = \left|\eta_{0,r}+\eta_{r-1,r}+(r-3)(\eta_{1,r}+\eta_{r-2,r})-(r-2)(\eta_{2,r}+\eta_{r-3,r})\right| \tag{64}$$

More specifically, the explicit form of ${\tau_{2r-1}}^{ho}$ for $r=5$ can be written by

$${\tau_9}^{ho} = \left|\eta_{0,5}+\eta_{4,5}+2(\eta_{1,5}+\eta_{3,5})-6\eta_{2,5}\right| \tag{65}$$

3.3.3. The optimal higher order ${\tau_{2r-1}}^{opt}$ ($r>3$)

Other than the aforementioned two kinds of approaches for developing the global smoothness indicator τ_{2r-1} by linear combinations of the local smoothness indicators, it is found that the order of the global smoothness indicator τ_{2r-1} can be raised to up to $O(\Delta x^{2r+2})$ by using instead of the local smoothness indicators but the derivatives of the Lagrangian interpolation polynomials directly. The optimal higher order ${\tau_{2r-1}}^{opt}$ is defined as

$${\tau_{2r-1}}^{opt} = \Delta x|F_1|\sum_{m=2}^{r-1}\Delta x^m|F_m|, \tag{66}$$

where F_m $(m=1,\ldots,r-1)$ are

$$F_1 = \begin{cases} |P^{(1)}_{i-r+1,r}(x_i)| - |P^{(1)}_{i,r}(x_i)| + (r-1)[|P^{(1)}_{i-r+2,r}(x_i)| - |P^{(1)}_{i-1,r}(x_i)|], & \mathrm{mod}\,(r,2)=0; \\ |P^{(1)}_{i-r+1,r}(x_i)| + |P^{(1)}_{i,r}(x_i)| + (r-3)[|P^{(1)}_{i-r+2,r}(x_i)| + |P^{(1)}_{i-1,r}(x_i)|] - (r-2)[|P^{(1)}_{i-r+3,r}(x_i)| + |P^{(1)}_{i-2,r}(x_i)|]|, & \\ \qquad\qquad \mathrm{mod}\,(r,2)=1 \end{cases} \tag{67}$$

$$F_m = \left|P^{(m)}_{i-r+1,r}(x_i)\right| - \left|P^{(m)}_{i,r}(x_i)\right|, \quad m>1 \tag{68}$$

From (36), (40) and (41), it is not difficult to verify that

$$O\left(\Delta x^m F_m\right) = \begin{cases} O(\Delta x^{r+2}), & m=1; \\ O(\Delta x^r), & m>1 \end{cases} \tag{69}$$

Therefore, the truncation error of ${\tau_{2r-1}}^{opt}$ is of the order $O(\Delta x^{2r+2})$.

Table 1
Rate of convergence at a second order critical point for WENO-Z and WENO-Zη schemes ($p = 2$).

N	WENO-Z		WENO-Z$\eta(\tau_7^{ho})$		WENO-Z$\eta(\tau_7^{opt})$	
	Error	Order	Error	Order	Error	Order
2^3	4.66E−02	–	4.77E−02	–	5.73E−03	–
2^4	5.76E−04	6.3	1.11E−03	5.4	3.49E−05	7.4
2^5	6.64E−06	6.4	2.38E−05	5.5	1.84E−08	10.9
2^6	2.50E−08	8.1	3.82E−07	6.0	1.47E−10	7.0
2^7	4.47E−10	5.8	5.02E−09	6.3	1.18E−12	7.0
2^8	6.38E−12	6.1	6.46E−11	6.3	–	–

Table 2
Rate of convergence at a second order critical point for WENO-Z and WENO-Zη schemes ($p = 1$).

N	WENO-Z		WENO-Z$\eta(\tau_7^{ho})$		WENO-Z$\eta(\tau_7^{opt})$	
	Error	Order	Error	Order	Error	Order
2^3	1.23E−02	–	1.37E−02	–	4.70E−03	–
2^4	9.01E−05	7.1	2.90E−04	5.6	1.32E−05	8.5
2^5	1.61E−06	5.8	6.36E−06	5.5	1.84E−08	9.5
2^6	5.61E−08	4.8	1.73E−07	5.2	1.47E−10	7.0
2^7	1.68E−09	5.1	5.09E−09	5.1	1.15E−12	7.0
2^8	5.04E−11	5.1	1.55E−10	5.0	–	

4. Convergence at the critical points

Critical points have become a focus of discussion since in [11] it was shown that the standard value of the parameter $\varepsilon = 10^{-6}$ in fact *hides* the loss of accuracy of fifth-order WENO-JS which achieves only third order at critical points of smooth solutions. WENO-M was presented as a *fix* to this situation, for it used a mapping that corrected the weights of WENO-JS and recovered the formal fifth-order at critical points even when using very small values of ε. Furthermore, it was demonstrated in [5] that the WENO-Z scheme can achieve the fifth-order convergence at first order critical points of a smooth solution provided the parameter p in (11) is taken as 2. As an advantage over these fifth-order WENO schemes, the WENO-Zη scheme is demonstrated to be able to keep the fifth-order convergence rate even at the second order critical points of a smooth solution [8].

In this paper, we will verify that the maximum-order convergence rate of the high order WENO-Zη scheme can also be realized at the second order critical points of a smooth solution with aid of the optimized global smoothness indicator ${\tau_{2r-1}}^{opt}$. For sake of brevity, only the case of $r = 4$ is examined in this section. We now perform numerical experiments to compare behaviors of the WENO-Z and WENO-Zη in the presence of smooth solutions containing critical points.

Consider the following test function

$$f(x) = x^k \exp(x), \quad x \in [-1, 1], \tag{70}$$

which has a critical point of order $n_{cp} = k - 1$ at $x = 0$. In other word, the first $k - 1$ derivatives of this function $f^{(j)}(0) = 0$, $j = 0, 1, \ldots, k - 1$. Tables 1 and 2 show the L_∞ convergence behaviors of these schemes at the second order critical points ($k = 3$). As shown in Tables 1 and 2, decreasing value of p from 2 to 1 incurs the convergence rate of WENO-Z and WENO-Z$\eta(\tau_7^{ho})$ dropping from 6th-order to 5th-order, while, the convergence rate of WENO-Z$\eta(\tau_7^{opt})$ keeping at 7th-order.

5. Numerical examples

In this section, performances of WENO-η and WENO-$Z\eta$ will be examined and compared with the classic schemes. The numerical presentation of this section starts with the solution of the one dimensional Euler equations with Riemann initial value problems such as the Lax, Sod, shock-density wave interaction and the interacting blast problems, and followed by the two dimensional problems on the double-Mach shock reflection and forward facing step problems. The time dependent problems are all solved via the 3rd-order Runge–Kutta TVD method [16] with CFL = 0.5.

5.1. 1D Euler systems

The one-dimensional Euler equations for gas dynamics in strong conservation form can be described by

$$\frac{\partial \mathbf{U}}{\partial t} + \frac{\partial \mathbf{F}}{\partial x} = 0, \tag{71}$$

where

$$\mathbf{U} = (\rho, \rho u, E)^T, \qquad \mathbf{F} = \left(\rho u, \rho u^2 + P, (E + P)u\right)^T \tag{72}$$

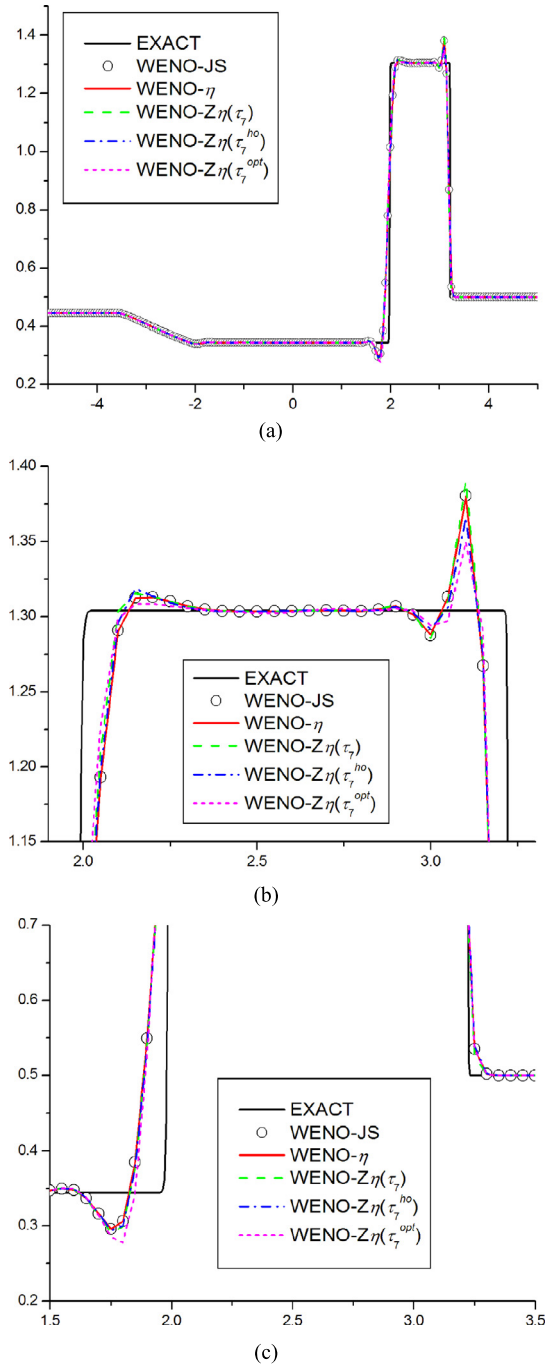

Fig. 2. Numerical solutions of the Lax problem as computed by the 7th-order WENO schemes with $N = 200$ at $t = 1.3$: (a) presents the comparison between the exact solution and the numerical results of WENO-JS, WENO-η, WENO-Z$\eta(\tau_7)$, WENO-Z$\eta({\tau_7}^{ho})$ and WENO-Z$\eta({\tau_7}^{opt})$; (b) and (c) are the local enlarged plots of (a).

The equation of state is given by

$$P = (\gamma - 1)\left(E - \frac{1}{2}\rho u^2\right), \quad \gamma = 1.4, \tag{73}$$

where ρ, u, P and E are the density, velocity, pressure and total energy, respectively. These equations are solved by following the general WENO methodology [12]. The numerical experiments are conducted using 200 grid points.

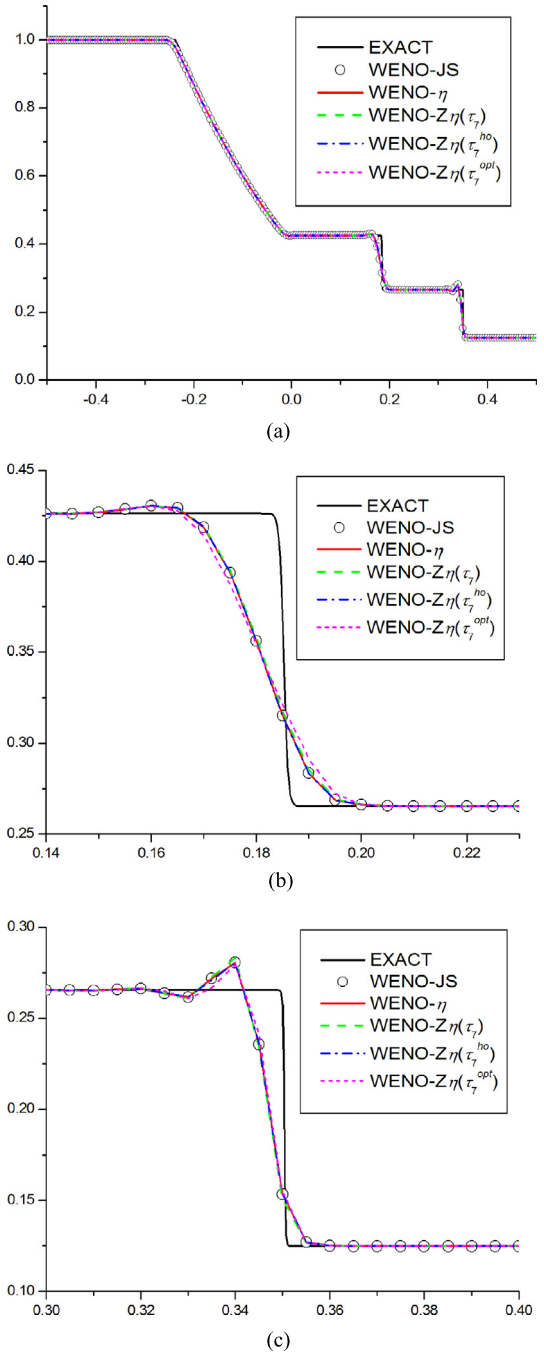

Fig. 3. Numerical solutions of the Sod problem as computed by the 7th-order WENO schemes with $N = 200$ at $t = 0.2$: (a) presents the comparison between the exact solution and the numerical results of WENO-JS, WENO-η, WENO-Z$\eta(\tau_7)$, WENO-Z$\eta({\tau_7}^{ho})$ and WENO-Z$\eta({\tau_7}^{opt})$; (b) and (c) are the local enlarged plots of (a).

5.1.1. Riemann initial value problem of Lax

For the Lax problem, the initial condition is

$$(\rho, U, p) = \begin{cases} (0.445, 0.698, 0.3528), & -5 \leqslant x < 0, \\ (0.5, 0, 0.571), & 0 \leqslant x \leqslant 5, \end{cases} \tag{74}$$

and the final time is 1.3. The densities that computed by the 7th-order WENO schemes ($r = 4$) are presented and shown in Fig. 2 in which the performances of WENO-JS, WENO-η, WENO-Z$\eta(\tau_7)$, WENO-Z$\eta({\tau_7}^{ho})$ and WENO-Z$\eta({\tau_7}^{opt})$ schemes are compared. We refer to the solution computed by the 5th-order WENO-JS scheme ($r = 3$) with $N = 4000$ grid points as the

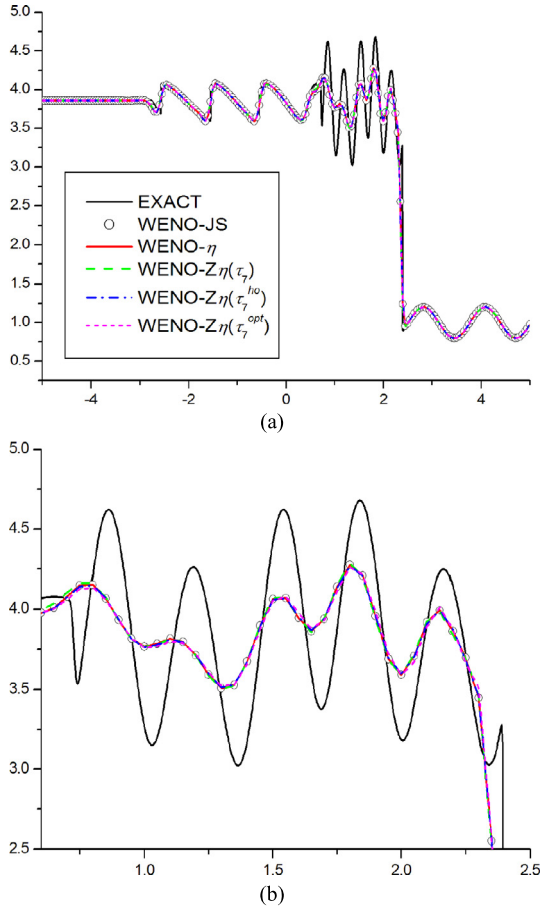

Fig. 4. Numerical solutions of the shock-density interaction as computed by the 7th-order WENO schemes with $N = 200$ at $t = 1.8$: (a) presents the comparison between the exact solution and the numerical results of WENO-JS, WENO-η, WENO-Z$\eta(\tau_7)$, WENO-Z$\eta({\tau_7}^{ho})$ and WENO-Z$\eta({\tau_7}^{opt})$; (b) is the local enlarged plot of (a).

'exact' solution. From Fig. 2, we see that all the results show oscillatory features near the discontinuities. In addition to this general observation, we can observe further that the results between WENO-η and WENO-JS are indistinguishable, while, WENO-$Z\eta(\tau_7)$ produces the strongest oscillations compared to the other WENO schemes.

5.1.2. Riemann initial value problem of Sod

For the Sod problem, the initial condition is

$$(\rho, U, p) = \begin{cases} (1.0, 0, 1.0), & x \leqslant 0, \\ (0.125, 0, 0.1), & x > 0, \end{cases} \tag{75}$$

and the final time is 0.2. The simulated density of Sod problem is shown in Fig. 3 where the results from various 7th-order WENO schemes are compared. It can be seen that all of numerical results agree well with each other except the most dissipative one computed by WENO-Z$\eta({\tau_7}^{opt})$.

5.1.3. Shock-density wave interaction

The initial condition for the shock-density wave interaction problem [16] is given by

$$(\rho, U, p) = \begin{cases} (3.857143, 2.629369, 10.3333), & x < -4, \\ (1 + 0.2\sin(5x), 0, 1.0), & x \geqslant -4 \end{cases} \tag{76}$$

This case represents a Mach 3 shock wave interacting a sine entropy wave. The results as computed by various 7th-order WENO schemes including the WENO-JS, WENO-η, WENO-Z$\eta(\tau_7)$, WENO-Z$\eta({\tau_7}^{ho})$ and WENO-Z$\eta({\tau_7}^{opt})$, at time $t = 1.8$ are plotted in Fig. 4. We can see that the differences between these 7th-order WENO schemes are quite indiscernible.

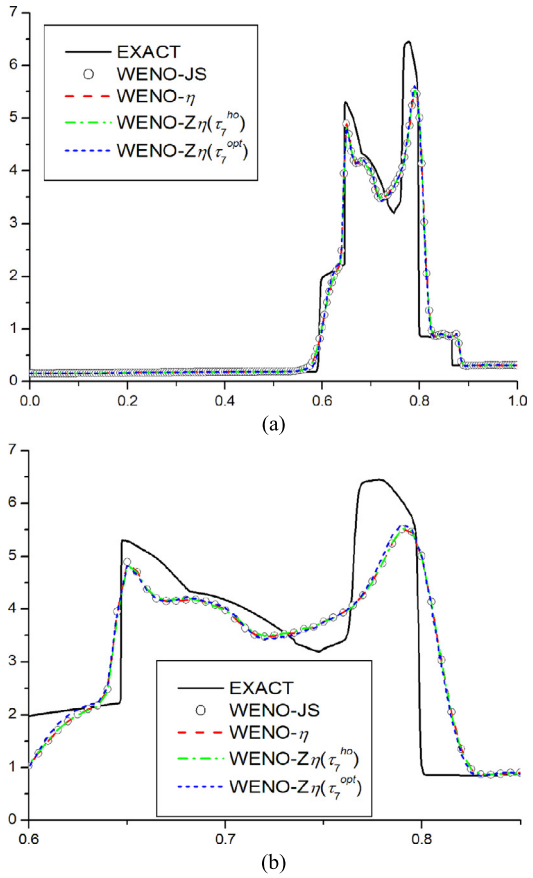

Fig. 5. Numerical solutions of the interacting blast waves problem as computed by the 7th-order WENO schemes with $N = 200$ at $t = 0.038$; (a) presents the comparison between the exact solution and the numerical results of WENO-JS, WENO-η, WENO-Z$\eta(\tau_7{}^{ho})$ and WENO-Z$\eta(\tau_7{}^{opt})$; (b) gives the local enlarged plot of (a).

5.1.4. Interacting blast wave problem

The initial condition for the interacting blast wave example [19] is

$$(\rho, U, p) = \begin{cases} (1, 0, 1000), & 0 \leqslant x < 0.1, \\ (1, 0, 0.01), & 0.1 \leqslant x < 0.9, \\ (1, 0, 100), & 0.9 \leqslant x \leqslant 1, \end{cases} \tag{77}$$

and the final time is 0.038. The results from four 7th-order WENO schemes, including the WENO-JS, WENO-η, WENO-Z$\eta(\tau_7{}^{ho})$ and WENO-Z$\eta(\tau_7{}^{opt})$, are presented in Fig. 5. As before, the differences between these 7th-order WENO schemes are insignificant. In addition, it should be mentioned that simulation was also run under the use of WENO-Z$\eta(\tau_7)$ scheme. However, the result was found to be unstable which may be ascribed to the less dissipative feature of the scheme.

5.2. 2D Euler systems

In this subsection, we extend the newly developed WENO-η and WENO-Zη schemes to solve the 2D compressible system of the form:

$$\frac{\partial \mathbf{U}}{\partial t} + \frac{\partial \mathbf{F}}{\partial x} + \frac{\partial \mathbf{G}}{\partial x} = 0, \tag{78}$$

where

$$\begin{aligned} \mathbf{U} &= (\rho, \rho u, \rho v, E)^T, \\ \mathbf{F} &= \left(\rho u, \rho u^2 + P, \rho uv, (E + P)u\right)^T, \\ \mathbf{G} &= \left(\rho v, \rho uv, \rho v^2 + P, (E + P)v\right)^T \end{aligned} \tag{79}$$

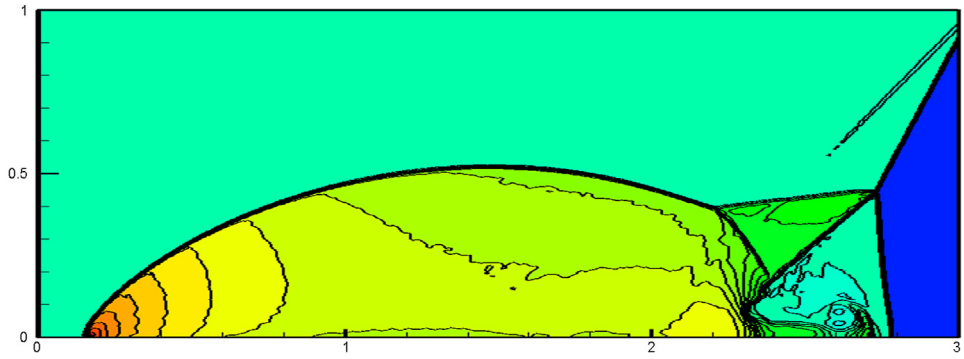

Fig. 6. Density contours of the double-Mach shock reflection as computed by the 7th-order WENO-η scheme ($r = 4$) at time $t = 0.2$. The mesh resolution is 800×200 zones and thirty contours were fit between a range of 1.3 and 22.

The equation of state is given by

$$P = (\gamma - 1)\left[E - \frac{1}{2}\rho\left(u^2 + v^2\right)\right], \quad \gamma = 1.4 \tag{80}$$

Here ρ, u, v, P and E are the density, components of velocity in the x and y coordinate directions, pressure and total energy, respectively. The Steger–Warming flux vector splitting method is used for the 2D problems in this paper.

5.2.1. Double Mach reflection of a strong shock

This problem has been carefully examined by Woodward and Colella [19]. We use the same setup as the authors did to test the problem where a Mach 10 shock hits a reflecting wall at the bottom of the domain given by $[0, 4] \times [0, 1]$. The angle between the shock and the horizontal axis is 60°. The equations are the two dimensional Euler equations ($\gamma = 1.4$) and initial conditions are

$$(\rho, u, v, p) = \begin{cases} (8, 8.25\cos\frac{\pi}{6}, -8.25\sin\frac{\pi}{6}, 116.5), & x < x_0 + \frac{y}{\sqrt{3}} \\ (1.4, 0, 0, 1.0), & x \geqslant x_0 + \frac{y}{\sqrt{3}} \end{cases} \tag{81}$$

with $x_0 = 1/6$. Boundary conditions at $x = 0$ are inflow, with post-shock values as above, and the right boundary is set to be outflow boundary. At $y = 0$, reflecting boundary conditions are applied to the interval $[x_0, 4]$. The top boundary condition imposes the exact motion of a Mach 10 shock in the flow variables.

Fig. 6 shows the density variable of the double-Mach shock reflection as computed by the 7th-order WENO-η scheme at $t = 0.2$ in $[0, 3] \times [0, 1]$ with a mesh resolution of 800×200. In Fig. 7 the density contours as computed by the various 7th-order WENO schemes ($r = 4$) including (a) WENO-JS, (b) WENO-η, (c) WENO-Z$\eta(\tau_7)$, (d) WENO-Z$\eta({\tau_7}^{ho})$ and (e) WENO-Z$\eta({\tau_7}^{opt})$ are compared. In order to observe more clearly the numerical solutions of the different WENO schemes, the region around the double Mach stems is displayed. In general, it can be found that the global structure of the solution is very similar across different schemes. However, the dissipation of the various schemes can be distinguished by the number of small vortices generated along the slip line and the wall jet behind the lower half of the right moving shock. As is clear in Fig. 7, the WENO-Z$\eta(\tau_7)$ shows the least dissipation, while, the dissipation of WENO-η is the strongest among these schemes.

Fig. 8 displays the density contours of the double-Mach shock reflection as computed by the 7th-order WENO-JS and WENO-η schemes under different mesh resolutions, which are 400×100 in (a) and $(a - 1)$, 800×200 in (b) and $(b - 1)$, and 1600×400 in (c) and $(c - 1)$, respectively. First of all, it can be observed that WENO-η shows the relatively stronger dissipation than WENO-JS. Furthermore, the details of small vortices along the slip line become increasingly apparent with the increase of the mesh resolution from 400×100 to 1600×400.

Fig. 9 presents the density contours of the double-Mach shock reflection as computed by the WENO-JS and WENO-η schemes with different orders of accuracy which are 5th-order in (a) and $(a - 1)$, 7th-order in (b) and $(b - 1)$, 9th-order in (c) and $(c - 1)$ and 11th-order in (d) and $(d - 1)$, respectively. It is quite as expected that much less dissipative results are produced by increasing order of accuracy of the schemes from 5th-order to 11th-order.

5.2.2. Forward facing step problem

This test problem was first presented by Woodward and Colella [19]. Recently, Balsara et al. [3] carried out a resolution study using the fourth order ADER-WENO scheme and showed that increasing the resolution enabled them to capture important details such as the roll-up of the vortex sheet via Kelvin–Helmholtz instability. In this paper, we also successfully captured the roll-up of the vortex sheet not only from increasing the grid resolution but also from using the new WENO-Zη schemes instead of the more dissipative WENO-JS and WENO-η. Furthermore, the robustness of the high order WENO-η scheme is supported by the success of simulating this severely stringent problem.

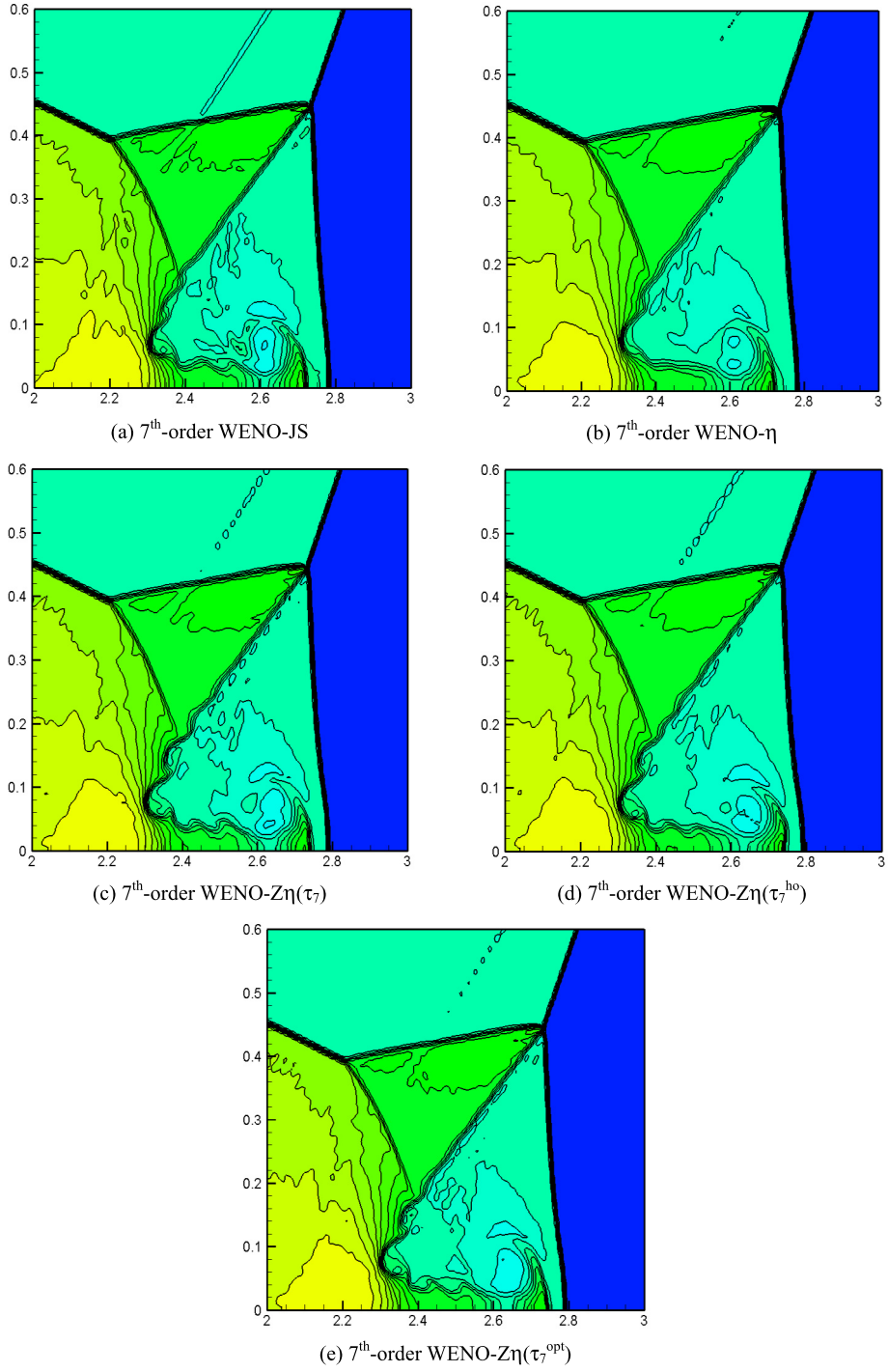

Fig. 7. Density contours of the double-Mach shock reflection as computed by the various 7th-order WENO schemes: (a) WENO-JS; (b) WENO-η; (c) WENO-Z$\eta(\tau_7)$; (d) WENO-Z$\eta(\tau_7{}^{ho})$ and (e) WENO-Z$\eta(\tau_7{}^{opt})$. The mesh resolution is 800×200 zones and thirty contours were fit between a range of 1.3 and 22.

The setup of this problem is the following: the wind tunnel spans a domain of $[0, 3] \times [0, 1]$. A forward-facing step is located at $(0.6, 0.2)$. The problem is initialized by a right-going Mach 3 flow with a density of 1.4 and a pressure of unity. Reflective boundary conditions are applied along the walls of the tunnel. Inflow and outflow boundary conditions are applied, respectively, at the left and right boundaries. The simulation was run until a time of 4 and the ratio of specific heats is given by 1.4.

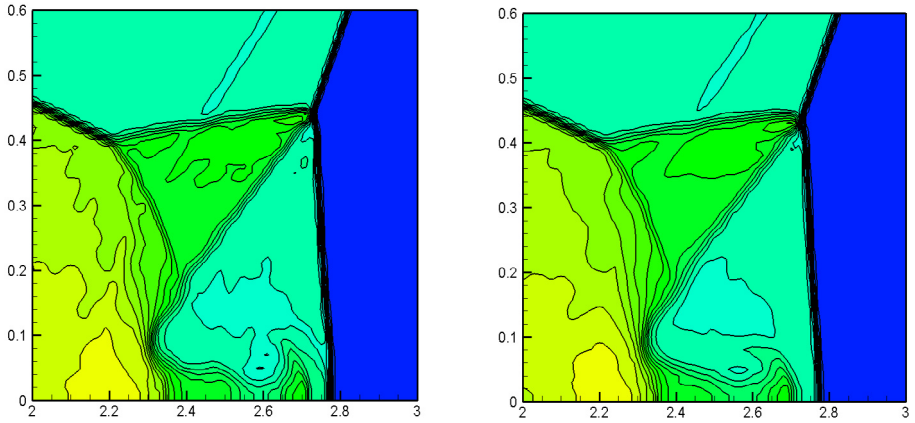

(a) 7th-order WENO-JS, mesh 400×100 (a-1) 7th-order WENO-η, mesh 400×100

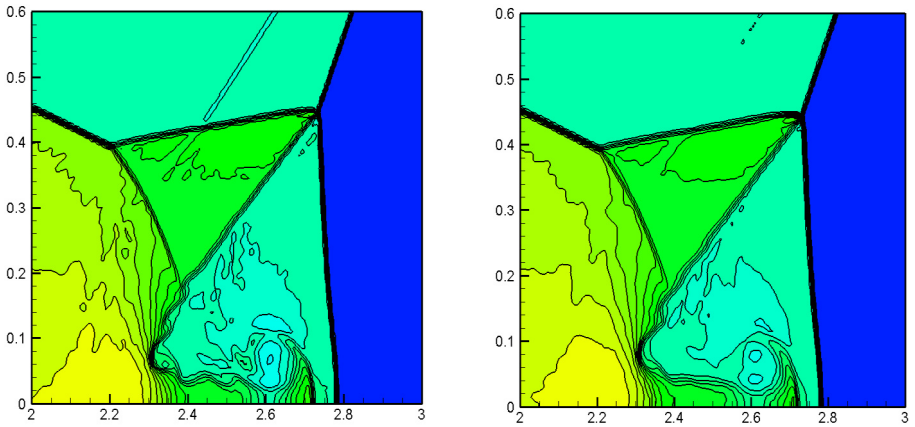

(b) 7th-order WENO-JS, mesh 800×200 (b-1) 7th-order WENO-η, mesh 800×200

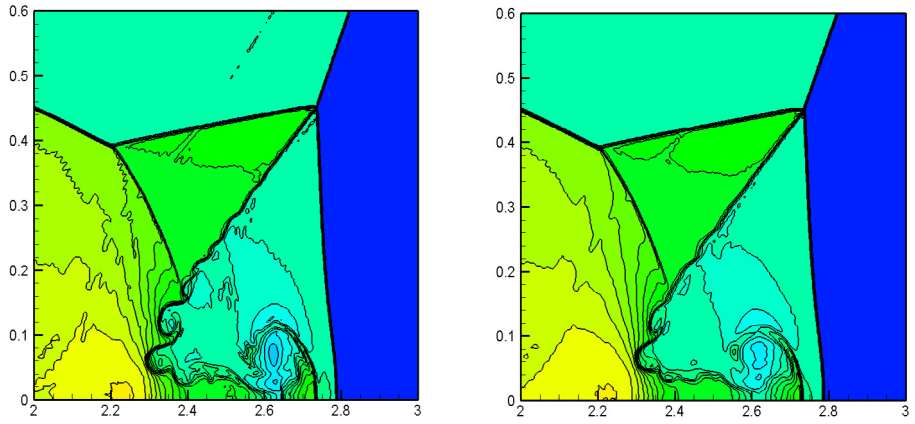

(c) 7th-order WENO-JS, mesh 1600×400 (c-1) 7th-order WENO-η, mesh 1600×400

Fig. 8. Density contours of the double-Mach shock reflection as computed by 7th-order WENO-JS and WENO-η schemes under different mesh resolutions which are 400×100 in (a) and $(a-1)$; 800×200 in (b) and $(b-1)$ and 1600×400 in (c) and $(c-1)$, respectively. Thirty contours were fit between a range of 1.3 and 22.

Fig. 10 shows the density as computed by the 7th-order WENO-η scheme at the final time in which the mesh resolutions are 300×100 in (a), 600×200 in (b) and 1200×400 in (c), respectively. It can be seen that all the shocks are found to have sharp profiles and captured properly on the computing grid. Furthermore, with the increase of the mesh resolution from 300×100 to 1200×400, the vortex sheets are observed more clearly that emanates from the Mach stem which agrees well with the result in [3].

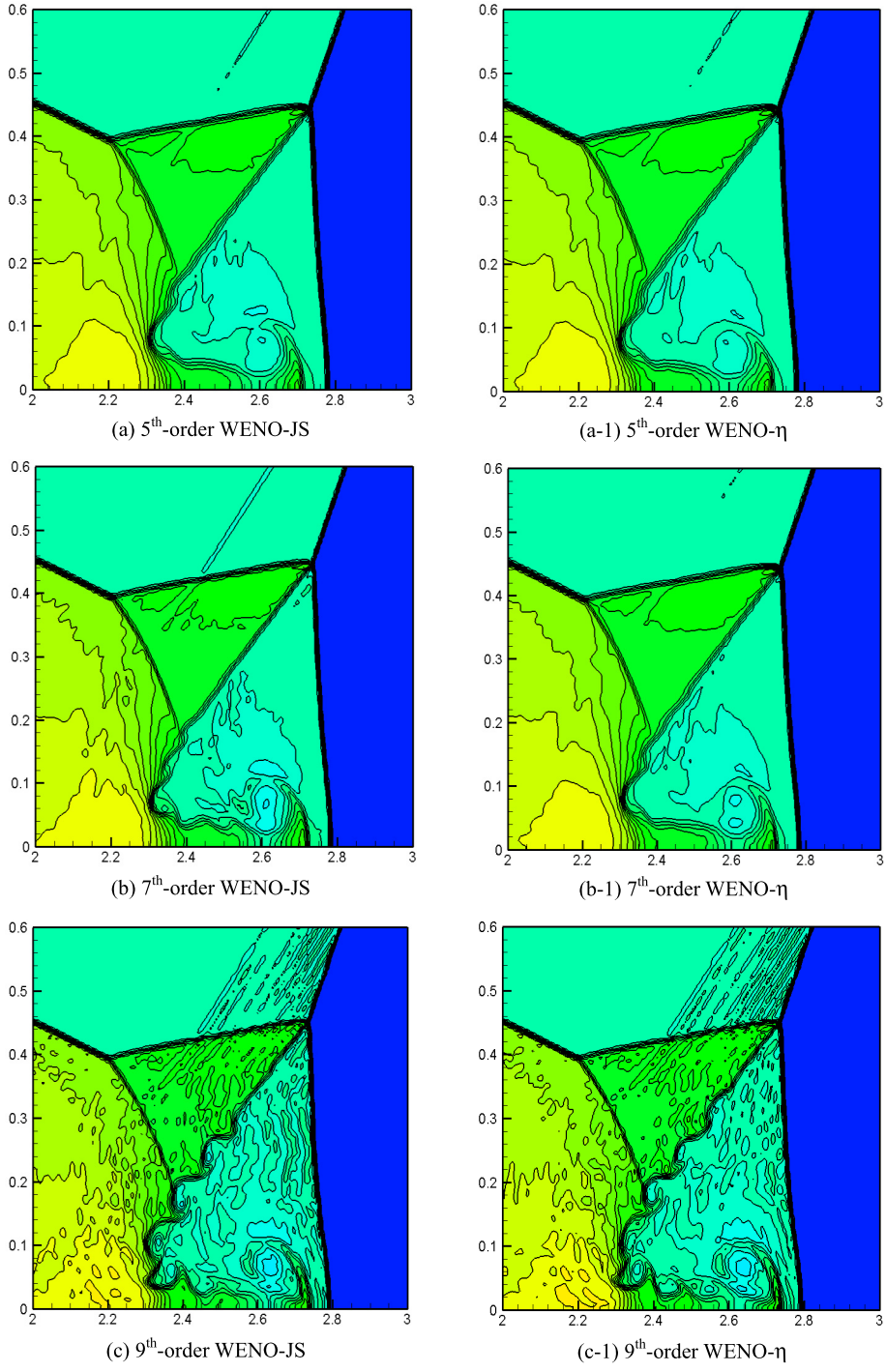

Fig. 9. Density contours of the double-Mach shock reflection as computed by the WENO-JS and WENO-η schemes with different orders of accuracy which are 5th-order in (a) and $(a-1)$; 7th-order in (b) and $(b-1)$; 9th-order in (c) and $(c-1)$ and 11th-order in (d) and $(d-1)$, respectively. The mesh resolution is 800×200 zones and thirty contours were fit between a range of 1.3 and 22.

Fig. 11 compares the results between various 7th-order WENO schemes including (a) WENO-JS; (b) WENO-η; (c) WENO-Z$\eta(\tau_7)$; (d) WENO-Z$\eta({\tau_7}^{ho})$ and (e) WENO-Z$\eta({\tau_7}^{opt})$ under a fixed mesh resolution 600×200. It is evident that the roll-up of the vortex sheet becomes much intense as the WENO-Z$\eta(\tau_7)$, WENO-Z$\eta({\tau_7}^{ho})$ and WENO-Z$\eta({\tau_7}^{opt})$ schemes are used, while, in a sharp contrast, the result of WENO-η shows the strongest dissipative feature.

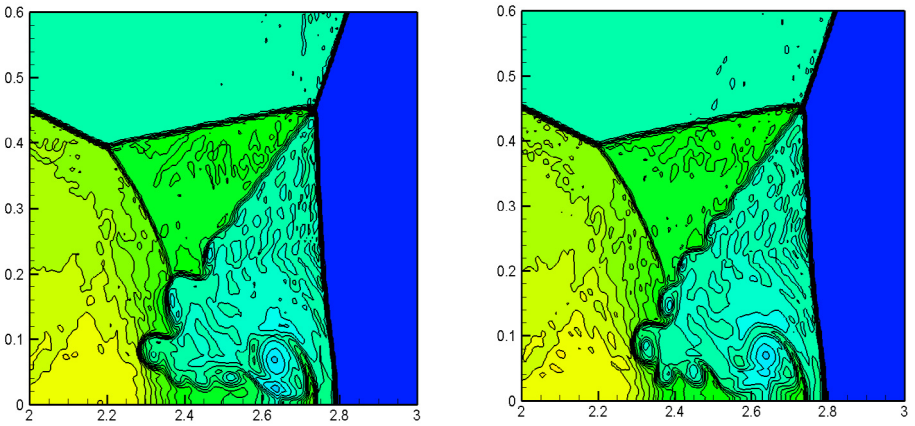

(d) 11th-order WENO-JS (d-1) 11th-order WENO-η

Fig. 9. (*continued*)

6. Conclusions

The fifth order WENO-η and WENO-Zη schemes introduced in [8] are extended to higher orders of accuracy by deriving the corresponding explicit expressions for the local smoothness indicator η and the global smoothness indicator τ. A thorough investigation is presented for the Taylor expansions of the Lagrangian interpolation polynomials and it is demonstrated that the Lagrangian interpolation bases of the local sub-stencils are symmetrical with respect to the global stencil. This gives the proof for the construction of τ_{2r-1} for all values of r, from linear combinations of η_l, or, using the derivatives of the Lagrangian interpolation polynomials directly. Closed-form formulae for the generation of the global smoothness indicators τ_{2r-1} are derived and the truncation error is optimized to $(2r+2)$th-order. Numerical experiments are run to show that the WENO-η scheme has a same good ENO property as or even better than the WENO-JS scheme in simulating the strong shock-capturing problems. The WENO-Zη scheme is less dissipative than WENO-η scheme and hence able to capture more details of the flow structures. On the other hand, the less dissipative property of the WENO-Zη scheme would make it unstable in simulating strong shocks problems.

Acknowledgements

This work is supported by NSFC (11172299). The helpful comments from the anonymous reviewers and the programs kindly provided by Prof. Y. Shen are also appreciated.

Appendix A. Taylor series expansion of the Lagrangian interpolation polynomial

The Lagrangian interpolation polynomial that approximates value of a smooth function $y(x)$ at any point x based upon a k-point stencil $S_{i,k}=\{x_i,\ldots,x_{i+k-1}\}$ can be written as

$$P_{i,k}(x)=\sum_{m=0}^{k-1} y_{i+m}\prod_{l=0,l\neq m}^{k-1}\frac{x-x_{i+l}}{x_{i+m}-x_{i+l}}, \tag{A.1}$$

where $y_i=y(x_i)$. The Taylor series expansions of the above expression about x for $k=1$, 2 and 3 are

$$P_{i,1}(x)=y_i=y(x)+(x_i-x)\sum_{l=1}^{\infty}\frac{y^{(l)}(x_i-x)^{l-1}}{l!} \tag{A.2}$$

$$P_{i,2}(x)=y(x)-(x_{i+1}-x)(x_i-x)\sum_{l=2}^{\infty}\frac{y^{(l)}}{l!}\frac{(x_{i+1}-x)^{l-1}-(x_i-x)^{l-1}}{x_{i+1}-x_i} \tag{A.3}$$

$$P_{i,3}(x)=y(x)+(x_{i+2}-x)(x_{i+1}-x)(x_i-x)\sum_{l=3}^{\infty}\frac{y^{(l)}}{l!}\frac{\frac{(x_{i+2}-x)^{l-1}-(x_{i+1}-x)^{l-1}}{x_{i+2}-x_{i+1}}-\frac{(x_{i+1}-x)^{l-1}-(x_i-x)^{l-1}}{x_{i+1}-x_i}}{x_{i+2}-x_i}, \tag{A.4}$$

which show evidently that the Lagrangian interpolation polynomials with $k=1$, $k=2$ and $k=3$ are first-order, second-order and third-order accurate, respectively.

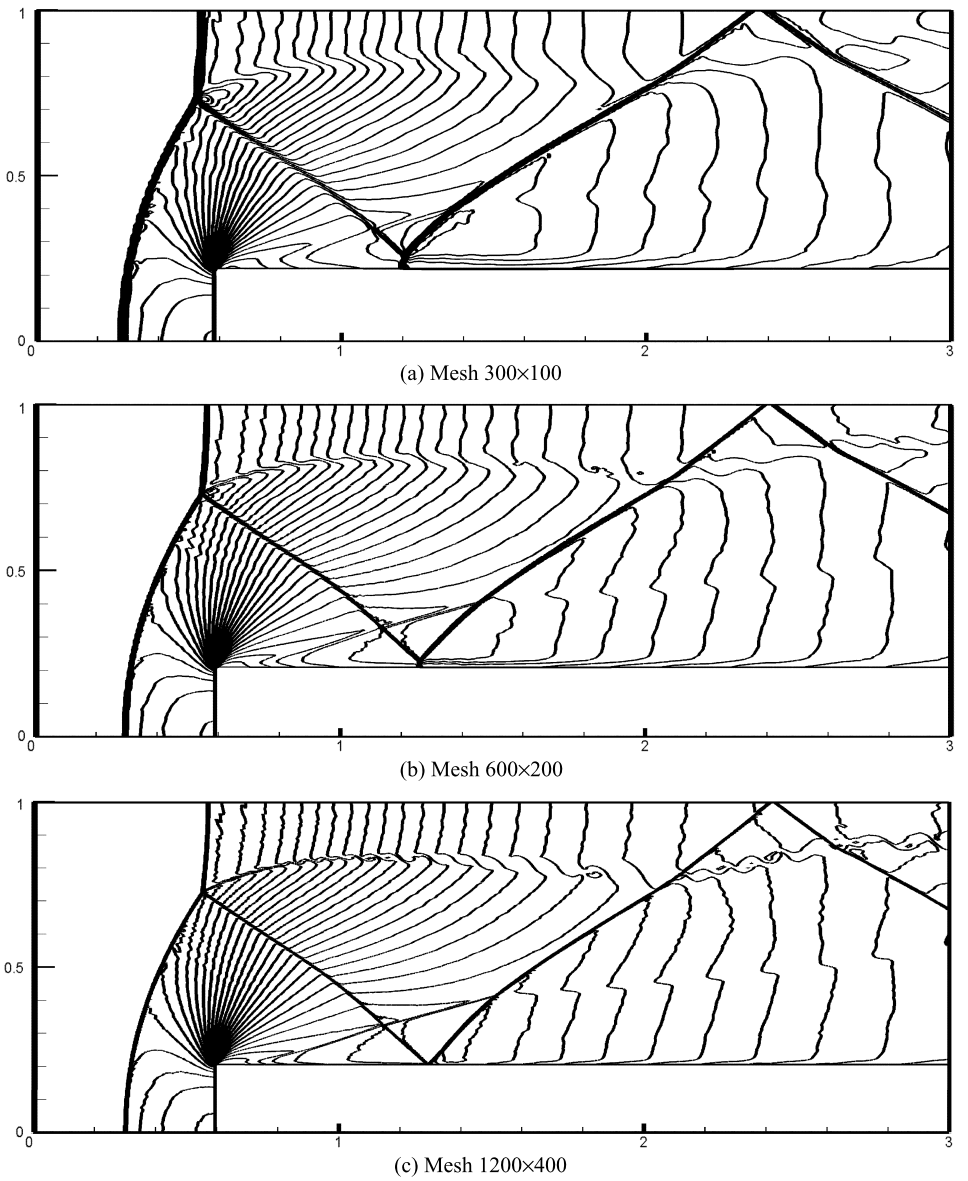

Fig. 10. Density contours of the forward facing step problem as computed by the 7th-order WENO-η scheme with different mesh resolutions: (a) 300×100; (b) 600×200; (c) 1200×400. Thirty equally spaced contours are shown ranging from 0.1 to 6.2.

From observing the second terms on RHS of the above equations, we are motivated to assume that the Lagrangian interpolation polynomial for arbitrary k can be expressed by the PSDD operator (see Appendix B), given by

$$P_{i,k}(x) = y(x) + (-1)^{k+1} \prod_{m=0}^{k-1} f_{i+m} \sum_{l=k}^{\infty} \frac{y^{(l)}}{l!}[l-1, i, k-1], \tag{A.5}$$

where the function that the PSDD operator acted on is defined by

$$f_i(x) = x_i - x \tag{A.6}$$

With aid of the property of PSDD operator given in (B.21), (A.5) can be rewritten as

$$P_{i,k}(x) = y(x) + (-1)^{k+1} \prod_{m=0}^{k-1} f_{i+m} \left(\frac{y^{(k)}}{k!} + \sum_{l=k+1}^{\infty} \frac{y^{(l)}}{l!}[l-1, i, k-1] \right) \tag{A.7}$$

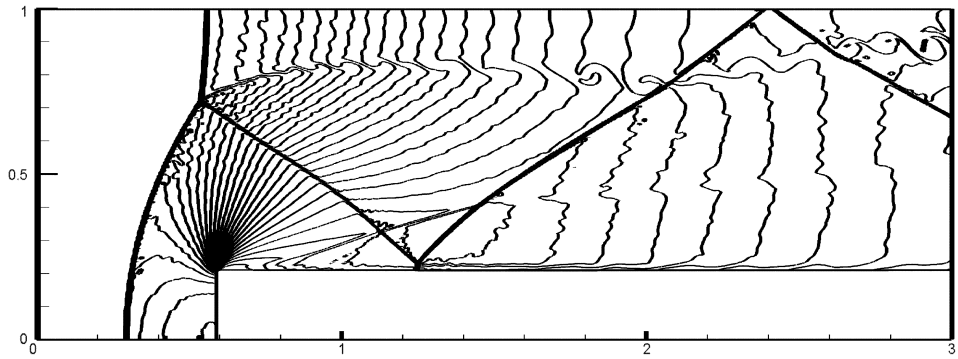

(a) WENO-JS

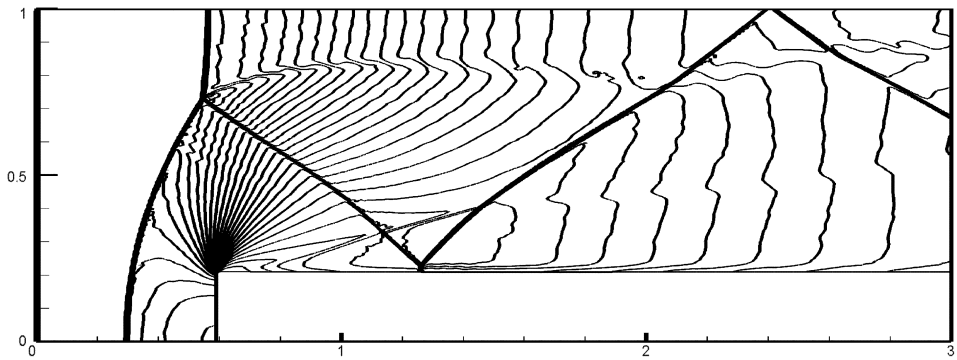

(b) WENO-η

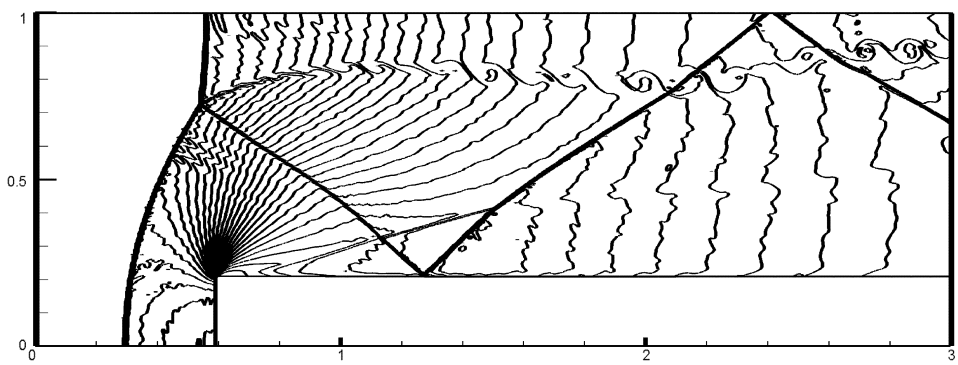

(c) WENO-Zη(τ_7)

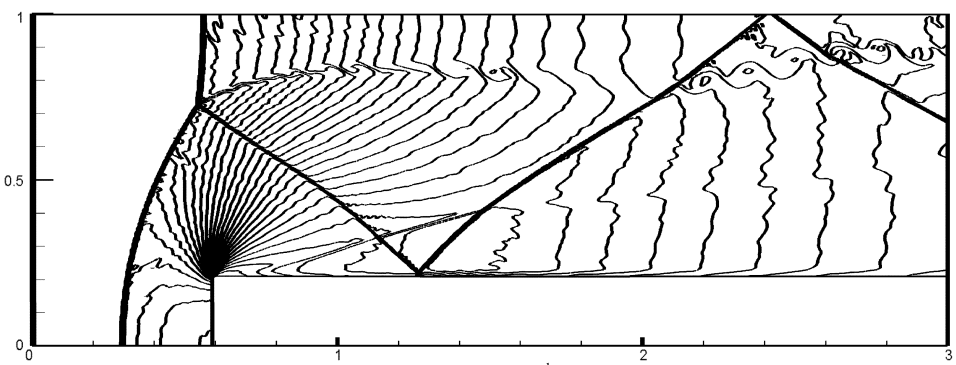

(d) WENO-Zη(τ_7^{ho})

Fig. 11. Density contours of the forward facing step problem as computed by the 7th-order WENO schemes: (a) WENO-JS; (b); WENO-η; (c) WENO-Z$\eta(\tau_7)$; (d) WENO-Z$\eta(\tau_7{}^{ho})$; (e) WENO-Z$\eta(\tau_7{}^{opt})$. The resolution is 600×200 zones and 30 equally spaced contours are shown ranging from 0.1 to 6.2.

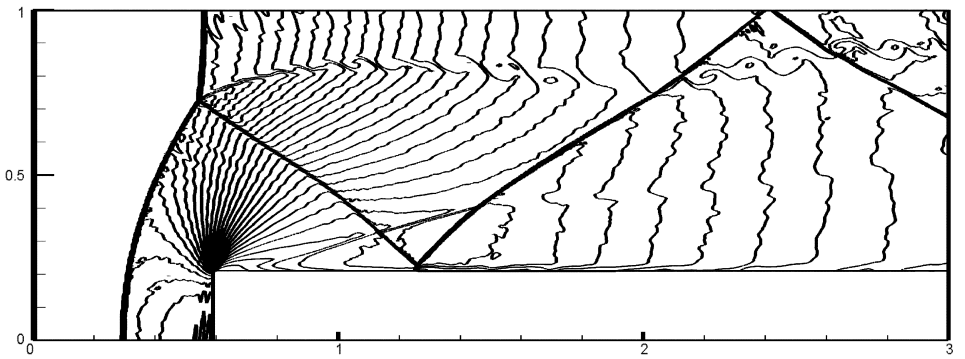

(e) WENO-Zη(τ_7^{opt})

Fig. 11. (*continued*)

Note that the Lagrangian interpolation polynomial has the following recursive relation, termed as the Neville–Aitken algorithm [17],

$$P_{i,k+1}(x) = \gamma_{i,k} P_{i,k}(x) + \widehat{\gamma}_{i,k} P_{i+1,k}(x), \tag{A.8}$$

with the fundamental weights given by

$$\gamma_{i,k} = \frac{x_{i+k} - x}{x_{i+k} - x_i}, \qquad \widehat{\gamma}_{i,k} = 1 - \gamma_{i,k} = \frac{x - x_i}{x_{i+k} - x_i} \tag{A.9}$$

By substituting (A.7) into (A.8) one can have

$$\begin{aligned} P_{i,k+1}(x) &= y(x) + (-1)^{k+1} \frac{x_{i+k} - x}{x_{i+k} - x_i} \prod_{m=0}^{k-1} f_{i+m} \left(\frac{y^{(k)}}{k!} + \sum_{l=k+1}^{\infty} \frac{y^{(l)}}{l!} [l-1, i, k-1] \right) \\ &\quad + (-1)^{k+1} \frac{x - x_i}{x_{i+k} - x_i} \prod_{m=0}^{k-1} f_{i+1+m} \left(\frac{y^{(k)}}{k!} + \sum_{l=k+1}^{\infty} \frac{y^{(l)}}{l!} [l-1, i+1, k-1] \right) \\ &= y(x) + (-1)^{k+2} \prod_{m=0}^{k} f_{i+m} \sum_{l=k+1}^{\infty} \frac{y^{(l)}}{l!} [l-1, i, k] \end{aligned} \tag{A.10}$$

The above equation shows clearly that the previously assumed expression for the Lagrangian interpolation polynomial of arbitrary k (A.5) has been proven successfully.

By using properties of PSDD operator in (B.19), (B.20) and (B.21), (A.5) can be rewritten as

$$P_{i,k}(x) = y(x) - \frac{y^{(k)}}{k!} \prod_{l=0}^{k-1} (x - x_{i+l}) + \frac{y^{(k+1)}}{(k+1)!} \sum_{l=0}^{k-1} (x - x_{i+l}) \prod_{m=0}^{k-1} (x - x_{i+m}) + O\left(\Delta x^{k+2}\right) \tag{A.11}$$

where Δx is the magnitude of $x - x_i$.

Appendix B. Power-self-divided-difference operator and its properties

To assist the Taylor series expansion for the Lagrangian interpolation polynomial, it is instructive to introduce a PSDD operator and discuss its properties. The PSDD operator on any real smooth function $f(x)$ is defined as

$$\begin{aligned} &f[n, i, 0] = f_i^n, \\ &f[n, i, 1] = \frac{f_{i+1}^n - f_i^n}{f_{i+1} - f_i}, \\ &\ldots; \\ &f[n, i, k] = \frac{[n, i+1, k-1] - [n, i, k-1]}{f_{i+l} - f_i}, \quad 2 \leqslant k \leqslant n \end{aligned} \tag{B.1}$$

Hereafter, we will omit f in the expression of PSDD for brevity.

It is not difficult to observe that for $n = 1$

$$[1, i, 1] = \frac{f_{i+1} - f_i}{f_{i+1} - f_i} = 1, \tag{B.2}$$

$n = 2$

$$[2, i, 1] = \frac{f_{i+1}^2 - f_i^2}{f_{i+1} - f_i} = \sum_{l=0}^{1} f_{i+l};$$

$$[2, i, 2] = \frac{[2, i+1, 1] - [2, i, 1]}{f_{i+2} - f_i} = \frac{\sum_{l=0}^{1} f_{i+1+l} - \sum_{l=0}^{1} f_{i+l}}{f_{i+2} - f_i} = 1, \tag{B.3}$$

and $n = 3$

$$[3, i, 2] = \frac{[3, i+1, 1] - [3, i, 1]}{f_{i+2} - f_i} = \frac{\frac{f_{i+2}^3 - f_{i+1}^3}{f_{i+2} - f_{i+1}} - \frac{f_{i+1}^3 - f_i^3}{f_{i+1} - f_i}}{f_{i+2} - f_i} = \sum_{l=0}^{2} f_{i+l};$$

$$[3, i, 3] = \frac{[3, i+1, 2] - [3, i, 2]}{f_{i+3} - f_i} = \frac{\sum_{l=0}^{2} f_{i+1+l} - \sum_{l=0}^{2} f_{i+l}}{f_{i+2} - f_i} = 1 \tag{B.4}$$

For $n > 3$, we can first expand the PSDD with $k = 1$ as

$$[n, i, 1] = \frac{f_{i+1}^n - f_i^n}{f_{i+1} - f_i} = \sum_{l_1=0}^{n-1} f_{i+1}^{l_1} f_i^{n-1-l_1} = \sum_{l_1=0}^{n-1} f_i^{l_1} f_{i+1}^{n-1-l_1} \tag{B.5}$$

Then, the expression of PSDD with $k = 2$ can be yielded, given by

$$\begin{aligned}[n, i, 2] &= \frac{[n, i+1, 1] - [n, i, 1]}{f_{i+2} - f_i} = \frac{\sum_{l_1=0}^{n-1} f_{i+2}^{l_1} f_{i+1}^{n-1-l_1} - \sum_{l_1=0}^{n-1} f_i^{l_1} f_{i+1}^{n-1-l_1}}{f_{i+2} - f_i} \\ &= \sum_{l_1=1}^{n-1} f_{i+1}^{n-1-l_1} \frac{f_{i+2}^{l_1} - f_i^{l_1}}{f_{i+2} - f_i}\end{aligned} \tag{B.6}$$

Note that the RHS of the above equation can be expanded, in a 'positive sequence' ('PS') form, as

$$\begin{aligned}\sum_{l_1=1}^{n-1} f_{i+1}^{n-1-l_1} \frac{f_{i+2}^{l_1} - f_i^{l_1}}{f_{i+2} - f_i} &= \sum_{l_1=1}^{n-1} f_{i+1}^{n-1-l_1} \sum_{l_2=0}^{l_1-1} f_i^{l_2} f_{i+2}^{l_1-1-l_2} \\ &= \sum_{l_1=1}^{n-1} \sum_{l_2=0}^{l_1-1} f_i^{l_2} f_{i+1}^{n-1-l_1} f_{i+2}^{l_1-1-l_2} \\ &= \sum_{l_2=0}^{n-2} \sum_{l_1=l_2+1}^{n-1} f_i^{l_2} f_{i+1}^{n-1-l_1} f_{i+2}^{l_1-1-l_2} \\ &= \sum_{l_2=0}^{n-2} \sum_{l_1=0}^{n-2-l_2} f_i^{l_2} f_{i+1}^{n-2-l_2-l_1} f_{i+2}^{l_1} \\ &= \sum_{l_2=0}^{n-2} \sum_{l_1=0}^{n-2-l_2} f_i^{l_2} f_{i+1}^{l_1} f_{i+2}^{n-2-l_2-l_1},\end{aligned} \tag{B.7}$$

or, alternatively, expanded into the following 'reverse sequence' ('RS') form

$$\begin{aligned}\sum_{l_1=1}^{n-1} f_{i+1}^{n-1-l_1} \frac{f_{i+2}^{l_1} - f_i^{l_1}}{f_{i+2} - f_i} &= \sum_{l_1=1}^{n-1} f_{i+1}^{n-1-l_1} \sum_{l_2=0}^{l_1-1} f_{i+2}^{l_2} f_i^{l_1-1-l_2} \\ &= \sum_{l_1=1}^{n-1} \sum_{l_2=0}^{l_1-1} f_{i+2}^{l_2} f_i^{l_1-1-l_2} f_{i+1}^{n-1-l_1}\end{aligned}$$

$$= \sum_{l_2=0}^{n-2} \sum_{l_1=l_2+1}^{n-1} f_{i+2}^{l_2} f_i^{l_1-1-l_2} f_{i+1}^{n-1-l_1}$$
$$= \sum_{l_2=0}^{n-2} \sum_{l_1=0}^{n-2-l_2} f_{i+2}^{l_2} f_i^{l_1} f_{i+1}^{n-2-l_2-l_1} \tag{B.8}$$

As a consequence, we can assume that the 'PS' and 'RS' forms of PSDD for $k > 2$ are expressed, respectively, as

$$[n,i,k]_+ = \sum_{l_k=0}^{n-k} \sum_{l_{k-1}=0}^{n-k-l_k} \cdots \sum_{l_1=0}^{n_s} \left[\left(\prod_{m=0}^{k-1} f_{i+m}^{l_{k-m}} \right) f_{i+k}^{n_s-l_1} \right] \tag{B.9}$$

$$[n,i,k]_- = \sum_{l_k=0}^{n-k} \sum_{l_{k-1}=0}^{n-k-l_k} \cdots \sum_{l_1=0}^{n_s} \left[f_{i+k}^{l_k} \left(\prod_{m=0}^{k-2} f_{i+m}^{l_{k-1-m}} \right) f_{i+k-1}^{n_s-l_1} \right], \tag{B.10}$$

in which the subscript "+" and "−" denote the 'PS' and 'RS' forms of PSDD, respectively, and n_s is defined by

$$n_s = n - k - \sum_{m=0}^{k-2} l_{k-m} \tag{B.11}$$

It follows immediately from (B.10) that

$$[n,i+1,k]_- = \sum_{l_k=0}^{n-k} \sum_{l_{k-1}=0}^{n-k-l_k} \cdots \sum_{l_1=0}^{n_s} \left[f_{i+k+1}^{l_k} \left(\prod_{m=0}^{k-2} f_{i+1+m}^{l_{k-1-m}} \right) f_{i+k}^{n_s-l_1} \right] \tag{B.12}$$

Then, from (B.9) and (B.12), one can have

$$[n,i,k+1] = \frac{[n,i+1,k]-[n,i,k]}{f_{i+k+1}-f_i} = \frac{[n,i+1,k]_- - [n,i,k]_+}{f_{i+k+1}-f_i}$$
$$= \sum_{l_k=1}^{n-k} \sum_{l_{k-1}=0}^{n-k-l_k} \cdots \sum_{l_1=0}^{n_s} \left[\left(\prod_{m=0}^{k-2} f_{i+1+m}^{l_{k-1-m}} \right) f_{i+k}^{n_s-l_1} \frac{f_{i+k+1}^{l_k} - f_i^{l_k}}{f_{i+k+1}-f_i} \right] \tag{B.13}$$

The above equation can be further expanded into the 'PS' form as

$$[n,i,k+1]_+ = \sum_{l_k=1}^{n-k} \sum_{l_{k-1}=0}^{n-k-l_k} \cdots \sum_{l_1=0}^{n_s} \left[\left(\prod_{m=0}^{k-2} f_{i+1+m}^{l_{k-1-m}} \right) f_{i+k}^{n_s-l_1} \sum_{l_{k+1}=0}^{l_k-1} f_i^{l_{k+1}} f_{i+k+1}^{l_k-1-l_{k+1}} \right]$$
$$= \sum_{l_{k+1}=0}^{l_k-1} \sum_{l_k=1}^{n-k} \sum_{l_{k-1}=0}^{n-k-l_k} \cdots \sum_{l_1=0}^{n_s} \left[f_i^{l_{k+1}} \left(\prod_{m=0}^{k-2} f_{i+1+m}^{l_{k-1-m}} \right) f_{i+k}^{n_s-l_1} f_{i+k+1}^{l_k-1-l_{k+1}} \right]$$
$$= \sum_{l_{k+1}=0}^{n-k-1} \sum_{l_k=l_{k+1}+1}^{n-k} \sum_{l_{k-1}=0}^{n-k-l_k} \cdots \sum_{l_1=0}^{n_s} \left[f_i^{l_{k+1}} \left(\prod_{m=0}^{k-2} f_{i+1+m}^{l_{k-1-m}} \right) f_{i+k}^{n_s-l_1} f_{i+k+1}^{l_k-1-l_{k+1}} \right]$$
$$= \sum_{l_{k+1}=0}^{n-k-1} \sum_{l_k=0}^{n-k-1-l_{k+1}} \cdots \sum_{l_1=0}^{n_t} \left[f_i^{l_{k+1}} \left(\prod_{m=0}^{k-2} f_{i+1+m}^{l_{k-1-m}} \right) f_{i+k}^{n_t-l_1} f_{i+k+1}^{l_k} \right], \tag{B.14}$$

where

$$n_t = n - k - 1 - \sum_{m=0}^{k-1} l_{k+1-m} \tag{B.15}$$

Note that (B.14) can be rewritten, by using an exchange algorithm on the power, as

$$
\begin{aligned}
[n,i,k+1]_+ &= \sum_{l_{k+1}=0}^{n-k-1}\sum_{l_k=0}^{n-k-1-l_{k+1}}\cdots\sum_{l_1=0}^{n_t}\left[f_i^{l_{k+1}}\left(\prod_{m=0}^{k-3}f_{i+1+m}^{l_{k-1-m}}\right)\left(f_{i+k-1}^{l_1}f_{i+k}^{n_t-l_1}\right)f_{i+k+1}^{l_k}\right]\\
&= \sum_{l_{k+1}=0}^{n-k-1}\sum_{l_k=0}^{n-k-1-l_{k+1}}\cdots\sum_{l_1=0}^{n_t}\left[f_i^{l_{k+1}}\left(\prod_{m=0}^{k-3}f_{i+1+m}^{l_{k-1-m}}\right)\left(f_{i+k-1}^{n_t-l_1}f_{i+k}^{l_1}\right)f_{i+k+1}^{l_k}\right]\\
&= \sum_{l_{k+1}=0}^{n-k-1}\sum_{l_k=0}^{n-k-1-l_{k+1}}\cdots\sum_{l_1=0}^{n_t}\left[f_i^{l_{k+1}}\left(\prod_{m=0}^{k-4}f_{i+1+m}^{l_{k-1-m}}\right)\left(f_{i+k-2}^{l_2}f_{i+k-1}^{n_t-l_1}\right)f_{i+k}^{l_1}f_{i+k+1}^{l_k}\right]\\
&= \sum_{l_{k+1}=0}^{n-k-1}\sum_{l_k=0}^{n-k-1-l_{k+1}}\cdots\sum_{l_1=0}^{n_t}\left[f_i^{l_{k+1}}\left(\prod_{m=0}^{k-4}f_{i+1+m}^{l_{k-1-m}}\right)\left(f_{i+k-2}^{n_t-l_1}f_{i+k-1}^{l_2}\right)f_{i+k}^{l_1}f_{i+k+1}^{l_k}\right]
\end{aligned}
\tag{B.16}
$$

Then, by applying continuously the exchange algorithm on the power, (B16) can be further rewritten as

$$
\begin{aligned}
[n,i,k+1]_+ &= \sum_{l_{k+1}=0}^{n-k-1}\sum_{l_k=0}^{n-k-1-l_{k+1}}\cdots\sum_{l_1=0}^{n_t}\left[f_i^{l_{k+1}}f_{i+1}^{n_t-l_1}\left(\prod_{m=0}^{k-2}f_{i+2+m}^{l_{k-1-m}}\right)f_{i+k+1}^{l_k}\right]\\
&= \sum_{l_{k+1}=0}^{n-k-1}\sum_{l_k=0}^{n-k-1-l_{k+1}}\cdots\sum_{l_1=0}^{n_t}\left[f_i^{l_{k+1}}f_{i+1}^{l_k}\left(\prod_{m=0}^{k-2}f_{i+2+m}^{l_{k-1-m}}\right)f_{i+k+1}^{n_t-l_1}\right]\\
&= \sum_{l_{k+1}=0}^{n-k-1}\sum_{l_k=0}^{n-k-1-l_{k+1}}\cdots\sum_{l_1=0}^{n_t}\left[\left(\prod_{m=0}^{k}f_{i+m}^{l_{k+1-m}}\right)f_{i+k+1}^{n_t-l_1}\right]
\end{aligned}
\tag{B.17}
$$

On the other hand, Eq. (B.13) can also be expanded into its 'RS' form, given by

$$
\begin{aligned}
[n,i,k+1]_- &= \sum_{l_k=1}^{n-k}\sum_{l_{k-1}=0}^{n-k-l_k}\cdots\sum_{l_1=0}^{n_s}\left[\left(\prod_{m=0}^{k-2}f_{i+1+m}^{l_{k-1-m}}\right)f_{i+k}^{n_s-l_1}\sum_{l_{k+1}=0}^{l_k-1}f_{i+k+1}^{l_{k+1}}f_i^{l_k-1-l_{k+1}}\right]\\
&= \sum_{l_{k+1}=0}^{l_k-1}\sum_{l_k=1}^{n-k}\sum_{l_{k-1}=0}^{n-k-l_k}\cdots\sum_{l_1=0}^{n_s}\left[f_{i+k+1}^{l_{k+1}}f_i^{l_k-1-l_{k+1}}\left(\prod_{m=0}^{k-2}f_{i+1+m}^{l_{k-1-m}}\right)f_{i+k}^{n_s-l_1}\right]\\
&= \sum_{l_{k+1}=0}^{n-k-1}\sum_{l_k=l_{k+1}+1}^{n-k}\cdots\sum_{l_1=0}^{n_s}\left[f_{i+k+1}^{l_{k+1}}f_i^{l_k-1-l_{k+1}}\left(\prod_{m=0}^{k-2}f_{i+1+m}^{l_{k-1-m}}\right)f_{i+k}^{n_s-l_1}\right]\\
&= \sum_{l_{k+1}=0}^{n-k-1}\sum_{l_k=0}^{n-k-1-l_{k+1}}\cdots\sum_{l_1=0}^{n_t}\left[f_{i+k+1}^{l_{k+1}}f_i^{l_k}\left(\prod_{m=0}^{k-2}f_{i+1+m}^{l_{k-1-m}}\right)f_{i+k}^{n_t-l_1}\right]\\
&= \sum_{l_{k+1}=0}^{n-k-1}\sum_{l_k=0}^{n-k-1-l_{k+1}}\cdots\sum_{l_1=0}^{n_t}\left[f_{i+k+1}^{l_{k+1}}\left(\prod_{m=0}^{k-1}f_{i+m}^{l_{k-m}}\right)f_{i+k}^{n_t-l_1}\right]
\end{aligned}
\tag{B.18}
$$

From the above two equations it is evident that the previously assumptions on the 'PS' and 'RS' forms of PSDD (B.9) and (B.10), have been proved completely.

Note that the general expressions for PSDD (B.9) and (B.10) can be simplified considerably under some special situation. Firstly, one can identified that the PSDD operator is in such a scale, written as

$$
[n,i,k]\sim O\left(f_i^{n-k}\right) \tag{B.19}
$$

Furthermore, by substituting $k=n-1$ into (B.9), the PSDD operator can be simplified to

$$
\begin{aligned}
[n,i,n-1] &= \sum_{l_{n-1}=0}^{1}\sum_{l_{n-2}=0}^{1-l_{n-1}}\cdots\sum_{l_1=0}^{1-l_{n-1}\cdots-l_2}\left(f_i^{l_{n-1}}f_{i+1}^{l_{n-2}}\cdots f_{i+k-1}^{l_2}f_{i+n-2}^{l_1}f_{i+n-1}^{1-l_{n-1}\cdots-l_1}\right)\\
&= \sum_{m=0}^{n-1}f_{i+m},
\end{aligned}
\tag{B.20}
$$

and a more succinct form for the PSDD operator with $k=n$ can be yielded from the above equation, given by

$$[n,i,n]=\frac{[n,i+1,n-1]-[n,i,n-1]}{f_{i+n}-f_i}=\frac{\sum_{m=0}^{n-1}f_{i+1+m}-\sum_{m=0}^{n-1}f_{i+m}}{f_{i+n}-f_i}=1 \tag{B.21}$$

Appendix C. Derivations of the explicit expressions of the local smoothness indicators η for $r=4$, 5 and 6

In this appendix, we shall present the derivations of the explicit expressions for the local smoothness indicators η for $r=4$, 5 and $r=6$ from the recursive relation (27). To begin with, it is helpful to present the explicit expressions of the derivatives of the Lagrangian interpolation polynomial ${P_{i-l,3}}^{(m)}(x_i)$ $(m=0,1,2;\ -3\leqslant l\leqslant 5)$ for $r=3$, which can be calculated from Eq. (A.1) directly, as below [Note that we use the expression ${P_{i,r}}^{(m)}$ to stand for ${P_{i,r}}^{(m)}(x_i)$ for brevity]:

$$\begin{aligned}
&P_{i-5,3}=6f_{i-5}-15f_{i-4}+10f_{i-3}; \qquad P_{i-4,3}=3f_{i-4}-8f_{i-3}+6f_{i-2};\\
&P_{i-3,3}=f_{i-3}-3f_{i-2}+3f_{i-1}; \qquad P_{i-2,3}=P_{i-1,3}=P_{i,3}=f_i;\\
&P_{i+1,3}=3f_{i+1}-3f_{i+2}+f_{i+3}; \qquad P_{i+2,3}=6f_{i+2}-8f_{i+3}+3f_{i+4};\\
&P_{i+3,3}=10f_{i+3}-15f_{i+4}+6f_{i+5}
\end{aligned} \tag{C.1}$$

$$P^{(1)}_{i-l,3}=\frac{1}{2\Delta x}\sum_{n=0}^{2}s^{(1)}_{n,l,3}f_{i+n-l}=\frac{1}{2\Delta x}\left(\mathbf{s}^{(1)}_{l,3}\right)(\mathbf{f}_{i-l})^T \tag{C.2}$$

$$P^{(2)}_{i-l,3}=\frac{1}{\Delta x^2}(f_i-2f_{i+1}+f_{i+2}), \tag{C.3}$$

where

$$\begin{aligned}
&\left(\mathbf{s}^{(1)}_{5,3}\right)=(7,-16,9); \qquad \left(\mathbf{s}^{(1)}_{4,3}\right)=(5,-12,7); \qquad \left(\mathbf{s}^{(1)}_{3,3}\right)=(3,-8,5);\\
&\left(\mathbf{s}^{(1)}_{2,3}\right)=(1,-4,3); \qquad \left(\mathbf{s}^{(1)}_{1,3}\right)=(-1,0,1); \qquad \left(\mathbf{s}^{(1)}_{0,3}\right)=(-3,4,-1);\\
&\left(\mathbf{s}^{(1)}_{-1,3}\right)=(-5,8,-3); \qquad \left(\mathbf{s}^{(1)}_{-2,3}\right)=(-7,12,-5); \qquad \left(\mathbf{s}^{(1)}_{-3,3}\right)=(-9,16,-7)
\end{aligned} \tag{C.4}$$

By using the recursive relation (27), one can derive favorably the following explicit expressions for the derivatives of the Lagrangian interpolation polynomials for $r=4$ from the above known results of $r=3$. The results for $r=4$ and $m=0$ are given by

$$P_{i-5,4}=\frac{x_{i-2}-x_i}{x_{i-2}-x_{i-5}}P_{i-5,3}+\frac{x_i-x_{i-5}}{x_{i-2}-x_{i-5}}P_{i-4,3}=-4f_{i-5}+15f_{i-4}-20f_{i-3}+10f_{i-2} \tag{C.5}$$

$$P_{i-4,4}=\frac{x_{i-1}-x_i}{x_{i-1}-x_{i-4}}P_{i-4,3}+\frac{x_i-x_{i-4}}{x_{i-1}-x_{i-4}}P_{i-3,3}=-f_{i-4}+4f_{i-3}-6f_{i-2}+4f_{i-1} \tag{C.6}$$

$$P_{i+1,4}=\frac{x_{i+4}-x_i}{x_{i+4}-x_{i+1}}P_{i+1,3}+\frac{x_i-x_{i+1}}{x_{i+4}-x_{i+1}}P_{i+2,3}=4f_{i+1}-6f_{i+2}+4f_{i+3}-f_{i+4} \tag{C.7}$$

$$P_{i+2,4}=\frac{x_{i+5}-x_i}{x_{i+5}-x_{i+2}}P_{i+2,3}+\frac{x_i-x_{i+2}}{x_{i+5}-x_{i+2}}P_{i+3,3}=10f_{i+2}-20f_{i+3}+15f_{i+4}-4f_{i+5}, \tag{C.8}$$

and those for $r=4$ and $m=1$

$$P^{(1)}_{i-l,4}=\frac{x_{i+3-l}-x_i}{x_{i+3-l}-x_{i-l}}P^{(1)}_{i-l,3}+\frac{x_i-x_{i-l}}{x_{i+3-l}-x_{i-l}}P^{(1)}_{i+1-l,3}+\frac{P_{i+1-l,3}-P_{i-l,3}}{x_{i+3-l}-x_{i-l}}=\frac{1}{6\Delta x}\sum_{n=0}^{3}s^{(1)}_{n,l,4}f_{i+n-l}, \tag{C.9}$$

where

$$\begin{aligned}
&\left(\mathbf{s}^{(1)}_{n,5,4}\right)=(-26,93,-114,47); \qquad \left(\mathbf{s}^{(1)}_{n,4,4}\right)=(-11,42,-57,26);\\
&\left(\mathbf{s}^{(1)}_{n,3,4}\right)=(-2,9,-18,11); \qquad \left(\mathbf{s}^{(1)}_{n,2,4}\right)=(1,-6,3,2);\\
&\left(\mathbf{s}^{(1)}_{n,1,4}\right)=(-2,-3,6,-1); \qquad \left(\mathbf{s}^{(1)}_{n,0,4}\right)=(-11,18,-9,2);\\
&\left(\mathbf{s}^{(1)}_{n,-1,4}\right)=(-26,57,-42,11); \quad \left(\mathbf{s}^{(1)}_{n,-2,4}\right)=(-47,114,-93,26),
\end{aligned} \tag{C.10}$$

those for $r=4$ and $m=2$

$$P^{(2)}_{i-l,4}=\frac{x_{i+3-l}-x_i}{x_{i+3-l}-x_{i-l}}P^{(2)}_{i-l,3}+\frac{x_i-x_{i-l}}{x_{i+3-l}-x_{i-l}}P^{(2)}_{i+1-l,3}+2\frac{P^{(1)}_{i+1-l,3}-P^{(1)}_{i-l,3}}{x_{i+3-l}-x_{i-l}}=\frac{1}{\Delta x^2}\sum_{n=0}^{3}s^{(2)}_{n,l,4}f_{i+n-l}, \tag{C.11}$$

where

$$\begin{aligned}
&\left(\mathbf{s}^{(2)}_{n,5,4}\right) = (-3, 10, -11, 4); \qquad \left(\mathbf{s}^{(2)}_{n,4,4}\right) = (-2, 7, -8, 3);\\
&\left(\mathbf{s}^{(2)}_{n,3,4}\right) = (-1, 4, -5, 2); \qquad \left(\mathbf{s}^{(2)}_{n,2,4}\right) = (0, 1, -2, 1);\\
&\left(\mathbf{s}^{(2)}_{n,1,4}\right) = (1, -2, 1, 0); \qquad \left(\mathbf{s}^{(2)}_{n,0,4}\right) = (2, -5, 4, -1);\\
&\left(\mathbf{s}^{(2)}_{n,-1,4}\right) = (3, -8, 7, -2); \qquad \left(\mathbf{s}^{(2)}_{n,-2,4}\right) = (4, -11, 10, -3),
\end{aligned} \tag{C.12}$$

and those for $r = 4$ and $m = 3$ are

$$P^{(3)}_{i-l,4} = 3\frac{P^{(2)}_{i+1-l,3} - P^{(2)}_{i-l,3}}{x_{i+3-l} - x_{i-l}} = \frac{1}{\Delta x^3}\sum_{n=0}^{3} s^{(3)}_{n,l,4} f_{i+n-l}; \quad -2 \leqslant l \leqslant 5, \tag{C.13}$$

where

$$\left(\mathbf{s}^{(3)}_{n,l,4}\right) = (-1, 3, -3, 1) \tag{C.14}$$

Thus, the explicit forms for the local smoothness indicators $\eta_{l,4}$ can be calculated from the following formulation,

$$\eta_{l,4} = \sum_{m=1}^{3}\left[\Delta x^m P^{(m)}_{i-3+l,4}\right]^2, \quad 0 \leqslant l \leqslant 3 \tag{C.15}$$

Similarly, one can derive, with the help of the recursive relation (27), the following results for $r = 5$ from the above known results of $r = 4$. The results for $r = 5$ and $m = 0$ are given by

$$P_{i-5,5} = \frac{x_{i-1} - x_i}{x_{i-1} - x_{i-5}} P_{i-5,4} + \frac{x_i - x_{i-5}}{x_{i-1} - x_{i-5}} P_{i-4,4} = f_{i-5} - 5f_{i-4} + 10f_{i-3} - 10f_{i-2} + 5f_{i-1} \tag{C.16}$$

$$P_{i+1,5} = \frac{x_{i+5} - x_i}{x_{i+5} - x_{i+1}} P_{i+1,4} + \frac{x_i - x_{i+1}}{x_{i+5} - x_{i+1}} P_{i+2,4} = 5f_{i+1} - 10f_{i+2} + 10f_{i+3} - 5f_{i+4} + f_{i+5}, \tag{C.17}$$

and those for $r = 5$ and $m = 1$

$$\begin{aligned}
P^{(1)}_{i-l,5} &= \frac{x_{i+4-l} - x_i}{x_{i+4-l} - x_{i-l}} P^{(1)}_{i-l,4} + \frac{x_i - x_{i-l}}{x_{i+4-l} - x_{i-l}} P^{(1)}_{i+1-l,4} + \frac{P_{i+1-l,4} - P_{i-l,4}}{x_{i+4-l} - x_{i-l}}\\
&= \frac{1}{12\Delta x^2}\sum_{n=0}^{4} s^{(1)}_{n,l,5} f_{i+n-l},
\end{aligned} \tag{C.18}$$

where

$$\begin{aligned}
&\left(\mathbf{s}^{(1)}_{n,5,5}\right) = (25, -122, 234, -214, 77); \qquad \left(\mathbf{s}^{(1)}_{n,4,5}\right) = (3, -16, 36, -48, 25);\\
&\left(\mathbf{s}^{(1)}_{n,3,5}\right) = (-1, 6, -18, 10, 3); \qquad \left(\mathbf{s}^{(1)}_{n,2,5}\right) = (1, -8, 0, 8, -1);\\
&\left(\mathbf{s}^{(1)}_{n,1,5}\right) = (-3, -10, 18, -6, 1); \qquad \left(\mathbf{s}^{(1)}_{n,0,5}\right) = (-25, 48, -36, 16, -3);\\
&\left(\mathbf{s}^{(1)}_{n,-1,5}\right) = (-77, 214, -234, 122, -25),
\end{aligned} \tag{C.19}$$

those for $r = 5$ and $m = 2$

$$\begin{aligned}
P^{(2)}_{i-l,5} &= \frac{x_{i+4-l} - x_i}{x_{i+4-l} - x_{i-l}} P^{(2)}_{i-l,4} + \frac{x_i - x_{i-l}}{x_{i+4-l} - x_{i-l}} P^{(2)}_{i+1-l,4} + 2\frac{P^{(1)}_{i+1-l,4} - P^{(1)}_{i-l,4}}{x_{i+4-l} - x_{i-l}}\\
&= \frac{1}{12\Delta x^2}\sum_{n=0}^{4} s^{(2)}_{n,l,5} f_{i+n-l},
\end{aligned} \tag{C.20}$$

where

$$\begin{aligned}
&\left(\mathbf{s}^{(2)}_{n,5,5}\right) = (35, -164, 294, -236, 71); \qquad \left(\mathbf{s}^{(2)}_{n,4,5}\right) = (11, -56, 114, -104, 35);\\
&\left(\mathbf{s}^{(2)}_{n,3,5}\right) = (-1, 4, 6, -20, 11); \qquad \left(\mathbf{s}^{(2)}_{n,2,5}\right) = (-1, 16, -30, 16, -1);\\
&\left(\mathbf{s}^{(2)}_{n,1,5}\right) = (11, -20, 6, 4, -1); \qquad \left(\mathbf{s}^{(2)}_{n,0,5}\right) = (35, -104, 114, -56, 11);\\
&\left(\mathbf{s}^{(2)}_{n,-1,5}\right) = (71, -236, 294, -164, 35),
\end{aligned} \tag{C.21}$$

those for $r=5$ and $m=3$

$$P_{i-l,5}^{(3)} = \frac{x_{i+4-l}-x_i}{x_{i+4-l}-x_{i-l}} P_{i-l,4}^{(3)} + \frac{x_i-x_{i-l}}{x_{i+4-l}-x_{i-l}} P_{i+1-l,4}^{(3)} + 3\frac{P_{i+1-l,4}^{(2)} - P_{i-l,4}^{(2)}}{x_{i+4-l}-x_{i-l}}$$
$$= \frac{1}{2\Delta x^3} \sum_{n=0}^{4} s_{n,l,5}^{(3)} f_{i+n-l}, \tag{C.22}$$

where

$$\begin{aligned}
&\left(\mathbf{s}_{n,5,5}^{(3)}\right) = (5,-22,36,-26,7); \qquad \left(\mathbf{s}_{n,4,5}^{(3)}\right) = (3,-14,24,-18,5);\\
&\left(\mathbf{s}_{n,3,5}^{(3)}\right) = (1,-6,12,-10,3); \qquad \left(\mathbf{s}_{n,2,5}^{(3)}\right) = (-1,2,0,-2,1);\\
&\left(\mathbf{s}_{n,1,5}^{(3)}\right) = (-3,10,-12,6,-1); \qquad \left(\mathbf{s}_{n,0,5}^{(3)}\right) = (-5,18,-24,14,-3);\\
&\left(\mathbf{s}_{n,-1,5}^{(3)}\right) = (-7,26,-36,22,-5),
\end{aligned} \tag{C.23}$$

and those for $r=5$ and $m=4$ are

$$P_{i-l,5}^{(4)} = 4\frac{P_{i+1-l,4}^{(3)} - P_{i-l,4}^{(3)}}{x_{i+4-l}-x_{i-l}} = \frac{1}{\Delta x^4} \sum_{n=0}^{4} s_{n,l,5}^{(4)} f_{i+n-l}; \quad -1 \leqslant l \leqslant 5, \tag{C.24}$$

where

$$\left(\mathbf{s}_{n,l,5}^{(4)}\right) = (1,-4,6,-4,1) \tag{C.25}$$

Then, the explicit forms for the local smoothness indicators $\eta_{l,5}$ can be calculated from the following formulation

$$\eta_{l,5} = \sum_{m=1}^{4} \left[\Delta x^m P_{i-4+l,5}^{(m)}\right]^2, \quad 0 \leqslant l \leqslant 4 \tag{C.26}$$

The results for $r=6$ can be obtained recursively in a similar way. Specifically, the results for $r=6$ and $m=1$ are given by

$$P_{i-l,6}^{(1)} = \frac{x_{i+5-l}-x_i}{x_{i+5-l}-x_{i-l}} P_{i-l,5}^{(1)} + \frac{x_i-x_{i-l}}{x_{i+5-l}-x_{i-l}} P_{i+1-l,5}^{(1)} + \frac{P_{i+1-l,5} - P_{i-l,5}}{x_{i+5-l}-x_{i-l}}$$
$$= \frac{1}{60\Delta x^3} \sum_{n=0}^{5} s_{n,l,6}^{(1)} f_{i+n-l}, \tag{C.27}$$

where

$$\begin{aligned}
&\left(\mathbf{s}_{n,5,6}^{(1)}\right) = (-12,75,-200,300,-300,137);\\
&\left(\mathbf{s}_{n,4,6}^{(1)}\right) = (3,-20,60,-120,65,12);\\
&\left(\mathbf{s}_{n,3,6}^{(1)}\right) = (-2,15,-60,20,30,-3);\\
&\left(\mathbf{s}_{n,2,6}^{(1)}\right) = (3,-30,-20,60,-15,2);\\
&\left(\mathbf{s}_{n,1,6}^{(1)}\right) = (-12,-65,120,-60,20,-3);\\
&\left(\mathbf{s}_{n,0,6}^{(1)}\right) = (-137,300,-300,200,-75,12),
\end{aligned} \tag{C.28}$$

and those for $r=6$ and $m=2$

$$P_{i-l,6}^{(2)} = \frac{x_{i+5-l}-x_i}{x_{i+5-l}-x_{i-l}} P_{i-l,5}^{(2)} + \frac{x_i-x_{i-l}}{x_{i+5-l}-x_{i-l}} P_{i+1-l,5}^{(2)} + 2\frac{P_{i+1-l,5}^{(1)} - P_{i-l,5}^{(1)}}{x_{i+5-l}-x_{i-l}}$$
$$= \frac{1}{12\Delta x^3} \sum_{n=0}^{5} s_{n,l,6}^{(2)} f_{i+n-l}, \tag{C.29}$$

where

$$\left(\mathbf{s}^{(2)}_{n,5,6}\right) = (-10, 61, -156, 214, -154, 45); \qquad \left(\mathbf{s}^{(2)}_{n,4,6}\right) = (1, -6, 14, -4, -15, 10);$$
$$\left(\mathbf{s}^{(2)}_{n,3,6}\right) = (0, -1, 16, -30, 16, -1); \qquad \left(\mathbf{s}^{(2)}_{n,2,6}\right) = (-1, 16, -30, 16, -1, 0);$$
$$\left(\mathbf{s}^{(2)}_{n,1,6}\right) = (10, -15, -4, 14, -6, 1); \qquad \left(\mathbf{s}^{(2)}_{n,0,6}\right) = (45, -154, 214, -156, 61, -10), \tag{C.30}$$

those for $r = 6$ and $m = 3$

$$P^{(3)}_{i-l,6} = \frac{x_{i+5-l} - x_i}{x_{i+5-l} - x_{i-l}} P^{(3)}_{i-l,5} + \frac{x_i - x_{i-l}}{x_{i+5-l} - x_{i-l}} P^{(3)}_{i+1-l,5} + 3\frac{P^{(2)}_{i+1-l,5} - P^{(2)}_{i-l,5}}{x_{i+5-l} - x_{i-l}}$$
$$= \frac{1}{4\Delta x^3} \sum_{n=0}^{5} s^{(3)}_{n,l,6} f_{i+n-l}, \tag{C.31}$$

where

$$\left(\mathbf{s}^{(3)}_{n,5,6}\right) = (-7, 41, -98, 118, -71, 17); \qquad \left(\mathbf{s}^{(3)}_{n,4,6}\right) = (-1, 7, -22, 34, -25, 7);$$
$$\left(\mathbf{s}^{(3)}_{n,3,6}\right) = (1, -7, 14, -10, 1, 1); \qquad \left(\mathbf{s}^{(3)}_{n,2,6}\right) = (-1, -1, 10, -14, 7, -1);$$
$$\left(\mathbf{s}^{(3)}_{n,1,6}\right) = (-7, 25, -34, 22, -7, 1); \quad \left(\mathbf{s}^{(3)}_{n,0,6}\right) = (-17, 71, -118, 98, -41, 7), \tag{C.32}$$

those for $r = 6$ and $m = 4$

$$P^{(4)}_{i-l,6} = \frac{x_{i+5-l} - x_i}{x_{i+5-l} - x_{i-l}} P^{(4)}_{i-l,5} + \frac{x_i - x_{i-l}}{x_{i+5-l} - x_{i-l}} P^{(4)}_{i+1-l,5} + 4\frac{P^{(3)}_{i+1-l,5} - P^{(3)}_{i-l,5}}{x_{i+5-l} - x_{i-l}}$$
$$= \frac{1}{\Delta x^4} \sum_{n=0}^{5} s^{(4)}_{n,l,6} f_{i+n-l}, \tag{C.33}$$

where

$$\left(\mathbf{s}^{(4)}_{n,5,6}\right) = (-2, 11, -24, 26, -14, 3); \qquad \left(\mathbf{s}^{(4)}_{n,4,6}\right) = (-1, 6, -14, 16, -9, 2);$$
$$\left(\mathbf{s}^{(4)}_{n,3,6}\right) = (0, 1, -4, 6, -4, 1); \qquad \left(\mathbf{s}^{(4)}_{n,2,6}\right) = (1, -4, 6, -4, 1, 0);$$
$$\left(\mathbf{s}^{(4)}_{n,1,6}\right) = (2, -9, 16, -14, 6, -1); \qquad \left(\mathbf{s}^{(4)}_{n,0,6}\right) = (3, -14, 26, -24, 11, -2), \tag{C.34}$$

those for $r = 6$ and $m = 5$ are

$$P^{(5)}_{i-l,6} = 5\frac{P^{(4)}_{i+1-l,5} - P^{(4)}_{i-l,5}}{x_{i+5-l} - x_{i-l}} = \frac{1}{\Delta x^5} \sum_{n=0}^{5} s^{(5)}_{n,l,6} f_{i+n-l}; \quad 0 \leqslant l \leqslant 5, \tag{C.35}$$

where

$$\left(\mathbf{s}^{(5)}_{n,l,6}\right) = (-1, 5, -10, 10, -5, 1) \tag{C.36}$$

Then, the explicit forms for the local smoothness indicators $\eta_{l,6}$ can be calculated from the following formulation

$$\eta_{l,6} = \sum_{m=1}^{5} \left[\Delta x^m P^{(m)}_{i-5+l,6}\right]^2, \quad 0 \leqslant l \leqslant 5 \tag{C.37}$$

References

[1] D. Balsara, C.-W. Shu, Monotonicity preserving weighted essentially non-oscillatory schemes with increasingly high order of accuracy, J. Comput. Phys. 160 (2000) 405–452.
[2] D.S. Balsara, Divergence-free reconstruction of magnetic fields and WENO schemes for magnetohydrodynamics, J. Comput. Phys. 228 (2009) 5040–5056.
[3] D.S. Balsara, T. Rumpf, M. Dumbser, C.-D. Munz, Efficient, high-accuracy ADER-WENO schemes for hydrodynamics and divergence-free magnetohydrodynamics, J. Comput. Phys. 228 (2009) 2480–2516.
[4] D.S. Balsara, M. Dumbser, C. Meyer, H. Du, Z. Xu, Efficient implementation of ADER schemes for Euler and magnetohydrodynamic flow on structured meshes – comparison with Runge–Kutta methods, J. Comput. Phys. 235 (2013) 934–969.
[5] R. Borges, M. Carmona, B. Costa, W.S. Don, An improved weighted essentially non-oscillatory scheme for hyperbolic conservation laws, J. Comput. Phys. 227 (2008) 3101–3211.
[6] M. Castro, B. Costa, W.S. Don, High order weighted essentially non-oscillatory WENO-Z schemes for hyperbolic conservation laws, J. Comput. Phys. 230 (2011) 1766–1792.

[7] M. Dumbser, M. Käser, Arbitrary high order non-oscillatory finite volume schemes on unstructured meshes for linear hyperbolic systems, J. Comput. Phys. 221 (2007) 693–723.
[8] P. Fan, Y.Q. Shen, B.L. Tian, C. Yang, A new smoothness indicator for improving the weighted essentially nonoscillatory scheme, J. Comput. Phys. 269 (2014) 329–354, http://dx.doi.org/10.1016/j.jcp.2014.03.032.
[9] G.A. Gerolymos, D. Schal, I. Vallet, Very high order WENO schemes, J. Comput. Phys. 228 (2009) 8481–8524.
[10] A. Harten, B. Engquist, S. Osher, S. Chakravarthy, Uniformly high order essentially non-oscillatory schemes, III, J. Comput. Phys. 71 (1987) 231–303.
[11] A.K. Henrick, T.D. Aslam, J.M. Powers, Mapped weighted essentially non-oscillatory schemes: achieving optimal order near critical points, J. Comput. Phys. 207 (2005) 542–567.
[12] G.S. Jiang, C.-W. Shu, Efficient implementation of weighted ENO schemes, J. Comput. Phys. 126 (1996) 202–228.
[13] D. Levy, G. Puppo, G. Russo, Compact central WENO schemes for multidimensional conservation laws, SIAM J. Sci. Comput. 22 (2000) 656–672.
[14] X.D. Liu, S. Osher, T. Chan, Weighted essentially non-oscillatory schemes, J. Comput. Phys. 115 (1994) 200–212.
[15] C.-W. Shu, High order weighted essentially non-oscillatory schemes for convection dominated problems, SIAM Rev. 51 (2009) 82–126.
[16] C.-W. Shu, S. Osher, Efficient implementation of essentially non-oscillatory shock-capturing schemes, J. Comput. Phys. 77 (1988) 439–471.
[17] G.M. Phillips, Interpolation and Approximation by Polynomials, Springer, ISBN 0-387-00215-4, 2003, pp. 8–9.
[18] Y.-T. Zhang, C.-W. Shu, Third order WENO scheme on three dimensional tetrahedral meshes, Commun. Comput. Phys. 5 (2009) 836–848.
[19] P. Woodward, P. Colella, The numerical simulation of two-dimensional fluid flow with strong shocks, J. Comput. Phys. 54 (1984) 115–173.